The operating diagram for a two-step anaerobic digestion model.

Tewfik Sari, Boumediene Benyahia

Nonlinear Dynamics manuscript No.
(will be inserted by the editor)

The operating diagram for a two-step anaerobic digestion model

Tewfik Sari · Boumediene Benyahia

Received: date / Accepted: date

Abstract The Anaerobic Digestion Model ADM1 is a complex model which is widely accepted as a common platform for anaerobic process modeling and simulation. However, it has a large number of parameters and states that hinder its analytic study. Here, we consider the two-step simple model of anaerobic digestion named AM2, which is a four-dimensional system of ordinary differential equations. The AM2 model is able to adequately capture the main dynamical behavior of the full anaerobic digestion model ADM1 and has the advantage that a complete analysis for the existence and local stability of its steady states is available. We describe its operating diagram, which is the bifurcation diagram giving the behavior of the system with respect to the operating parameters, represented by the dilution rate and the input concentrations of the substrates. This diagram, is very useful to understand the model from both the mathematical and biological points of view. It is shown that six types of behavior can be obtained for the long-term dynamics of the AM2 model, concerning the coexistence or extinction of one or both bacterial populations.

Keywords Anaerobic digestion · ADM1 · AM2 model · Stability and Bifurcation · Operating diagram

Mathematics Subject Classification (2010) 37N25 · 92D25

T. Sari
ITAP, Univ Montpellier, INRAE, Institut Agro, Montpellier, France
E-mail: tewfik.sari@inrae.fr

B. Benyahia
Laboratoire d'Automatique de Tlemcen, Université de Tlemcen, Tlemcen, Algeria
E-mail: boumediene.benyahia@univ-tlemcen.dz

1 Introduction

The anaerobic digestion is a complex process in which organic material is converted into biogas, mainly composed of methane, in an environment without oxygen [4,8,26,32]. Anaerobic digestion enables the water industry to treat waste water as a resource for generating energy and recovering valuable by-products. The methane gas can be used as a renewable energy instead of fossil fuels. The complexity of the anaerobic digestion process has motivated the development of complex mathematical models, such as the widely used Anaerobic Digestion Model No. 1 (ADM1) [4]. The ADM1 system is a differential-algebraic equation system with 44 state variables (29 variables are of dynamic nature, and 15 variables are algebraic states) and more than 80 parameters. Since ADM1 is strongly non-linear and highly complex, it is impossible to obtain an analytical characterization of the steady states and to describe the operating diagram, that is to say, to identify the asymptotic behaviour of existing steady-states as a function of the operating parameters (substrates inflow concentrations and dilution rate). To the author's knowledge, for the ADM1 system, only numerical investigations are available [8].

Due to the analytic intractability of the full ADM1, work has been made towards the construction of simpler models that preserve biological meaning whilst reducing the computational effort required to find mathematical solutions of the model equations, to obtain a better understanding of the anaerobic digestion process. The simplest model of the chemostat with only one biological reaction, where one substrate is consumed by one microorganism is well understood [14,19,27]. However a one-step model is too simple to encapsulate the essence of the anaerobic digestion process.

More realistic models of anaerobic digestion are two-step models. An important contribution on the modelling of anaerobic digestion as a two-step is the model presented in [7], hereafter denoted as AM2 model, and studied in [6,25]. It has been shown that under some circumstances, this very simple two-step model is able to adequately capture the main dynamical behavior of the full anaerobic digestion model ADM1 [3,12]. Moreover, it has been shown that the simple AM2 model can support on-line control, optimization and supervision strategies, through the synthesis of state observers and control feedback laws [1,2].

Another simple two-step model of anaerobic digestion is the model presented in [35], where the product of the first microorganism, that serves as the substrate for the second microorganism, inhibits the growth of the first microorganism. The model incorporates a Monod with product inhibition kinetics for the first reaction and Monod kinetics alone for the second reaction term, and was extended with general growth functions characterized by qualitative properties in [10,23].

The two-step models studied in [6,7,25] present a commensalistic relationship between the microorganisms. According to [28], the commensalism is characterized by the fact that the second population (the commensal population) benefits for its growth from the first population (the host population) while the host population is not affected by the growth of the commensal population and hence, the first population can grow without the second one. On the contrary, the two-step models studied in [10,23,35] present a syntrophic relationship between the microorganisms: the first population is affected by the growth of the second population. For more details and information on commensalism and syntrophy, the reader is referred to [9,11,21,22,23,28, 30] and the references therein.

Another interesting simple anaerobic digestion models are the two-step models studied in [26,29], and the model with five state variables considered in [8,18]. We mention also the mathematical model, with eight state variables, which include syntrophy and substrate inhibition, considered in [33,34] and the mathematical model, with six state variables, which introduces an additional microorganism and substrate in a two-step syntrophic model, considered in [24,31].

In this paper we will consider the two-step AM2 model [6,7,25], and we describe its *operating diagram*. The operating diagram has the *operating parameters* as its coordinates and the various regions defined within it correspond to qualitatively different asymptotic behaviors. A two-step model has three operating parameters that are the input concentration of substrate for each reaction and the dilution rate. These parameters are *control parameters* since they are under the control of the experimenter. Apart from these three parameters, that can vary, all other parameters have biological meaning and are fitted using experimental data from ecological and/or biological observations of organisms and substrates.

Therefore the operating diagram is the bifurcation diagram that shows how the system behaves when we vary the control parameters. This diagram shows how extensive the parameter region is, where some asymptotic behaviors occur. This bifurcation diagram is very useful to understand the model from both the mathematical and biological points of view. Its importance for bioreactors was emphasized in [20], who attributed its introduction to [16], where the dynamics of predator and prey interactions is studied in a chemostat. This diagram is often constructed both in the biological literature [16,20,25,35,31] and the mathematical literature [8,10,17,23,24,29,33,34].

AM2 model can have up to six steady states. Its operating diagram was only partially described in [25], in the case $\alpha = 1$. In this paper we give a complete description of the diagram and, we show that it presents nine regions according to the number of steady states that can exist in each region, and the nature of their stability. The operating diagram summarizes the effect of the operating conditions on the long-term dynamics of the AM2 model and shows six types of behavior visualized in the figures by six different colors. Since AM2 model has three operating parameters, and it is not easy to visualize regions in the three-dimensional operating parameter space, two of the operating parameters are used as coordinates of the operating diagram and the effects of the third parameter are shown in a series of operating diagrams.

This paper is organized as follows: in section 2, we present the mathematical model and recall the necessary and sufficient conditions of existence of its steady states and their local, and global stability. Next, in section 3, we describe the operating diagram in the three-dimensional operating parameters space. In sections 4 and 5, we describe the operating diagrams in two-dimensional operating parameters space when the third operating parameter is kept fixed. In section 6, we present some bifurcation diagrams, with the dilution rate as the bifurcation parameter. Then, we conclude by discussing our results in section 7, before conclusions are formulated in the last section. Proofs, a Maple code to plot some figures of the paper, and Tables are given in the appendix.

Table 1 Auxiliary functions

$S_1^*(D)$	$S_1^*(D)$ is the unique solution of equation $\mu_1(S_1) = \alpha D$ It is defined for $0 \leq D < D_1$, where $D_1 = m_1/\alpha$ If $D \geq D_1$, by convention we let $S_1^*(D) = +\infty$
$S_2^{i*}(D)$, $i = 1, 2$	$S_2^{1*}(D) < S_2^{2*}(D)$ are the solutions of equation $\mu_2(S_2) = \alpha D$ They are defined for $0 \leq D \leq D_2$, where $D_2 = \mu_2(S_2^M)/\alpha$ If $D = D_2$, one has $S_2^{1*}(D) = S_2^{2*}(D)$ If $D > D_2$, by convention we let $S_2^{1*}(D) = +\infty$
$H_i(D)$, $i = 1, 2$	$H_i(D) = S_2^{i*}(D) + \frac{k_2}{k_1} S_1^*(D)$ It is defined for $0 \leq D < \min(D_1, D_2)$
$S_{2\text{in}}^*(D, S_{1\text{in}}, S_{2\text{in}})$	$S_{2\text{in}}^*(D, S_{1\text{in}}, S_{2\text{in}}) = S_{2\text{in}} + \frac{k_2}{k_1}(S_{1\text{in}} - S_1^*(D))$ It is defined for $0 \leq D < D_1$ and $S_{1\text{in}} > S_1^*(D)$
$X_1^*(D, S_{1\text{in}})$	$X_1^*(D, S_{1\text{in}}) = \frac{1}{k_1\alpha}(S_{1\text{in}} - S_1^*(D))$ It is defined for $0 \leq D < D_1$ and $S_{1\text{in}} > S_1^*(D)$
$X_2^i(D, S_{2\text{in}})$, $i = 1, 2$	$X_2^i(D, S_{2\text{in}}) = \frac{1}{k_3\alpha}(S_{2\text{in}} - S_2^{i*}(D))$ It is defined for $0 \leq D < D_2$ and $S_{2\text{in}} > S_2^{i*}(D)$
$X_2^{i*}(D, S_{1\text{in}}, S_{2\text{in}})$, $i = 1, 2$	$X_2^{i*}(D, S_{1\text{in}}, S_{2\text{in}}) = \frac{1}{k_3\alpha}(S_{2\text{in}}^*(D, S_{1\text{in}}, S_{2\text{in}}) - S_2^{i*}(D))$ It is defined for $0 \leq D < \min(D_1, D_2)$, $S_{1\text{in}} > S_1^*(D)$ and $S_{2\text{in}} + \frac{k_2}{k_1} S_{1\text{in}} > H_i(D)$

2 Mathematical model

We consider the AM2 model of anaerobic digestion given in [7], with a cascade of two biological reactions, where one substrate S_1 is degraded by one microorganism X_1 into a product S_2, that serves as the main limiting substrate for a second microorganism X_2

$$\begin{aligned} k_1 S_1 &\xrightarrow{\mu_1} X_1 + k_2 S_2 + k_4 \mathrm{CO}_2, \\ k_3 S_2 &\xrightarrow{\mu_2} X_2 + k_5 \mathrm{CO}_2 + k_6 \mathrm{CH}_4, \end{aligned} \tag{1}$$

where μ_1 and μ_2 are the kinetics of the reactions and k_i are pseudo-stoichiometric coefficients associated to the bioreactions. In the first step, the organic substrate S_1 is consumed by the acidogenic bacteria X_1 and produces a substrate S_2 (Volatile Fatty Acids), while, in the second step, the methanogenic population X_2 consumes S_2 and produces biogas. Let D be the dilution rate, $S_{1\text{in}}$ and $S_{2\text{in}}$ the concentrations of input substrates S_1 and S_2, respectively. The dynamical equations of the model take the form:

$$\begin{aligned} \dot{S}_1 &= D(S_{1\text{in}} - S_1) - k_1\mu_1(S_1)X_1, \\ \dot{X}_1 &= (\mu_1(S_1) - \alpha D)X_1, \\ \dot{S}_2 &= D(S_{2\text{in}} - S_2) + k_2\mu_1(S_1)X_1 - k_3\mu_2(S_2)X_2, \\ \dot{X}_2 &= (\mu_2(S_2) - \alpha D)X_2, \end{aligned} \tag{2}$$

where $\alpha \in [0, 1]$ is a parameter allowing us to decouple the HRT (Hydraulic Retention Time) and the SRT (Solid Retention Time). In [7], the kinetics μ_1 and μ_2 are of Monod and Haldane type, respectively:

$$\mu_1(S_1) = \frac{m_1 S_1}{K_1 + S_1}, \qquad \mu_2(S_2) = \frac{m_2 S_2}{K_2 + S_2 + \frac{S_2^2}{K_I}}. \tag{3}$$

The carbon dioxide and methane in (1) are outputs of the system, and have no feedback on the dynamical equations (2). In [3,26] this feedback, together with growth decay terms, are taken into consideration. Due to the cascade structure of the model (2), without added difficulty in the mathematical analysis, we can introduce decay terms in the removal rates of the bacteria, that is to say, we can replace αD by $\alpha D + a_i$, where a_i is the decay term for X_i, $i = 1, 2$.

Following [6,25], we will consider (2) with general $\mathcal{C}^1$ kinetics functions μ_1 and μ_2 satisfying the following qualitative properties:

Hypothesis 1 *$\mu_1(0) = 0$, $\mu_1(+\infty) = m_1$ and $\mu_1'(S_1) > 0$ for $S_1 > 0$.*

Hypothesis 2 *$\mu_2(0) = 0$, $\mu_2(+\infty) = 0$ and there exists $S_2^M > 0$ such that $\mu_2'(S_2) > 0$ for $0 < S_2 < S_2^M$, and $\mu_2'(S_2) < 0$ for $S_2 > S_2^M$.*

Table 2 The steady states of (2). S_1^*, S_2^{i*}, $i = 1, 2$, $S_{2\text{in}}^*$, X_1^*, X_2^i, $i = 1, 2$, and X_2^{i*}, $i = 1, 2$ are defined in Table 1.

E_1^0	$S_1 = S_{1\text{in}}$	$S_2 = S_{2\text{in}}$	$X_1 = 0$	$X_2 = 0$
E_1^i	$S_1 = S_{1\text{in}}$	$S_2 = S_2^{i*}$	$X_1 = 0$	$X_2 = X_2^i$
E_2^0	$S_1 = S_1^*$	$S_2 = S_{2\text{in}}^*$	$X_1 = X_1^*$	$X_2 = 0$
E_2^i	$S_1 = S_1^*$	$S_2 = S_2^{i*}$	$X_1 = X_1^*$	$X_2 = X_2^{i*}$

The system (2) can have at most six steady states, given in Table 2. For more details, the reader is referred to [6] and Appendix A. For the description of the steady states, we need to define the auxiliary functions S_1^*, $S_{2\text{in}}^*$, X_1^*, S_2^{i*} and X_2^{i*}, $i = 1, 2$, that are given in Table 1. For the particular case of Monod and Haldane functions (3), the auxiliary functions can be computed analytically and are given in Table 12. We have the following result.

Table 3 Necessary and sufficient conditions of existence and local stability of steady states of (2). $S_1^*(D)$, $S_2^{i*}(D)$, $i = 1, 2$, and $H_i(D)$, $i = 1, 2$, are defined in Table 1.

	Existence conditions	Stability conditions
E_1^0	Always exists	$S_{1\text{in}} < S_1^*(D)$ and $S_{2\text{in}} \notin [S_2^{1*}(D), S_2^{2*}(D)]$
E_1^1	$S_{2\text{in}} > S_2^{1*}(D)$	$S_{1\text{in}} < S_1^*(D)$
E_1^2	$S_{2\text{in}} > S_2^{2*}(D)$	Unstable if it exists
E_2^0	$S_{1\text{in}} > S_1^*(D)$	$S_{2\text{in}} + \frac{k_2}{k_1} S_{1\text{in}} \notin [H_1(D), H_2(D)]$
E_2^1	$S_{1\text{in}} > S_1^*(D)$ and $S_{2\text{in}} + \frac{k_2}{k_1} S_{1\text{in}} > H_1(D)$	Stable if it exists
E_2^2	$S_{1\text{in}} > S_1^*(D)$ and $S_{2\text{in}} + \frac{k_2}{k_1} S_{1\text{in}} > H_2(D)$	Unstable if it exists

Proposition 1 *Assume that Hypotheses 1 and 2 hold. The steady states E_1^0, E_1^i ($i = 1, 2$), E_2^0 and E_2^i ($i = 1, 2$) are given in Table 2. Their conditions of existence and stability are given in Table 3.*

Proof The proof is given in Appendix B.1. □

It should be noted that the steady states E_1^0 and E_2^0, where the methanogenic bacteria are washed out, produce no methane. The methane is produced when the system is functioning at the stable steady states E_1^1 or E_2^1, where the methanogenic bacteria are maintained. Although methane is produced by E_1^1, this requires extraneous addition of VFAs (the condition $S_{2\text{in}} > 0$ is necessary for the existence of E_1^1). Therefore, the steady state condition one would aim to achieve for stable operation is E_2^1, where all species survive and no extraneous addition of VFAs is required (the condition $S_{2\text{in}} = 0$ is compatible with the existence of E_2^1). However, it was shown that surprisingly, E_1^1 can be more productive in biogas than E_2^1 [5,34]. Therefore it is important for the experimenter to have a description of the regions of existence and stability of the steady states, given by the operating diagrams.

3 Operating diagram

The conditions $S_{1\text{in}} = S_1^*(D)$, $S_{2\text{in}} = S_2^{i*}(D)$, $i = 1, 2$, and $S_{1\text{in}} + \frac{k_2}{k_1} S_{2\text{in}} = H_i(D)$, $i = 1, 2$, in Table 3 define the boundaries in the operating parameter space where one of the steady states becomes positive or becomes stable. This suggests to define the surfaces Γ_i, $i = 1, \cdots, 6$, of Table 4. We have

$$\Gamma_1 = \{(D, S_{1\text{in}}, S_{2\text{in}}) : S_{1\text{in}} > 0 \text{ and } \alpha D = \mu_1(S_{1\text{in}})\}$$

$$\Gamma_2 \cup \Gamma_3 = \{(D, S_{1\text{in}}, S_{2\text{in}}) : S_{2\text{in}} > 0 \text{ and } \alpha D = \mu_2(S_{2\text{in}})\}$$

Notice that $S_2^{1*}(D) < S_2^{2*}(D)$ for $0 < D < D_2$ and equality holds for $D = D_2$. Similarly $H_1(D) < H_2(D)$ for $0 < D < \min(D_1, D_2)$, and equality holds for $D = \min(D_1, D_2)$. Therefore, the Γ_i surfaces separate the operating space $(D, S_{1\text{in}}, S_{2\text{in}})$ into nine regions, denoted $\mathcal{I}_k$, $k = 0, \cdots, 8$, and defined in Table 5. These regions of the operating parameters space $(D, S_{1\text{in}}, S_{2\text{in}})$ correspond to different system behaviors, as stated in the following result.

Table 4 The surfaces Γ_i, $i = 1, \cdots, 6$.

$$\Gamma_1 = \{(D, S_{1\text{in}}, S_{2\text{in}}) : 0 < D < D_1 \text{ and } S_{1\text{in}} = S_1^*(D)\}$$
$$\Gamma_2 = \{(D, S_{1\text{in}}, S_{2\text{in}}) : 0 < D < D_2 \text{ and } S_{2\text{in}} = S_2^{1*}(D)\}$$
$$\Gamma_3 = \{(D, S_{1\text{in}}, S_{2\text{in}}) : 0 < D < D_2 \text{ and } S_{2\text{in}} = S_2^{2*}(D)\}$$
$$\Gamma_4 = \{(D, S_{1\text{in}}, S_{2\text{in}}) : 0 < D < \min(D_1, D_2), S_{1\text{in}} > S_1^*(D) \text{ and } S_{2\text{in}} + \tfrac{k_2}{k_1} S_{1\text{in}} = H_1(D)\}$$
$$\Gamma_5 = \{(D, S_{1\text{in}}, S_{2\text{in}}) : 0 < D < \min(D_1, D_2), S_{1\text{in}} > S_1^*(D) \text{ and } S_{2\text{in}} + \tfrac{k_2}{k_1} S_{1\text{in}} = H_2(D)\}$$
$$\Gamma_6 = \{(D, S_{1\text{in}}, S_{2\text{in}}) : D = D_2 \text{ and } S_{2\text{in}} \geq S_2^M\}$$

Table 5 Definitions of the regions I_k, $k = 0, \cdots, 8$.

Region	Definition
$\mathcal{I}_0$	$S_{1\text{in}} < S_1^*(D)$ and $S_{2\text{in}} < S_2^{1*}(D)$
$\mathcal{I}_1$	$S_{1\text{in}} < S_1^*(D)$ and $S_2^{1*}(D) < S_{2\text{in}} \leq S_2^{2*}(D)$
$\mathcal{I}_2$	$S_{1\text{in}} < S_1^*(D)$ and $S_{2\text{in}} > S_2^{2*}(D)$
$\mathcal{I}_3$	$S_{1\text{in}} > S_1^*(D)$ and $S_{2\text{in}} + \frac{k_2}{k_1} S_{1\text{in}} < H_1(D)$
$\mathcal{I}_4$	$S_{1\text{in}} > S_1^*(D)$, $S_{2\text{in}} \leq S_2^{1*}(D)$ and $H_1(D) < S_{2\text{in}} + \frac{k_2}{k_1} S_{1\text{in}} \leq H_2(D)$
$\mathcal{I}_5$	$S_{1\text{in}} > S_1^*(D)$, $S_{2\text{in}} \leq S_2^{1*}(D)$ and $S_{2\text{in}} + \frac{k_2}{k_1} S_{1\text{in}} > H_2(D)$
$\mathcal{I}_6$	$S_{1\text{in}} > S_1^*(D)$, $S_{2\text{in}} > S_2^{1*}(D)$ and $S_{2\text{in}} + \frac{k_2}{k_1} S_{1\text{in}} \leq H_2(D)$
$\mathcal{I}_7$	$S_{1\text{in}} > S_1^*(D)$, $S_2^{1*}(D) < S_{2\text{in}} \leq S_2^{2*}(D)$ and $S_{2\text{in}} + \frac{k_2}{k_1} S_{1\text{in}} > H_2(D)$
$\mathcal{I}_8$	$S_{1\text{in}} > S_1^*(D)$ and $S_{2\text{in}} > S_2^{2*}(D)$

Proposition 2 *Assume that Hypotheses 1 and 2 hold. The existence and stability properties of the steady states of (2) are given in Table 6, where the regions $\mathcal{I}_k$, $k = 0, \cdots, 8$ are defined in Table 5.*

Proof The proof is given in Appendix B.2. □

Remark 1 *In Figs. 2, 3, 4, 5, 6 and 7 presenting operating diagrams, a region is colored according to the*

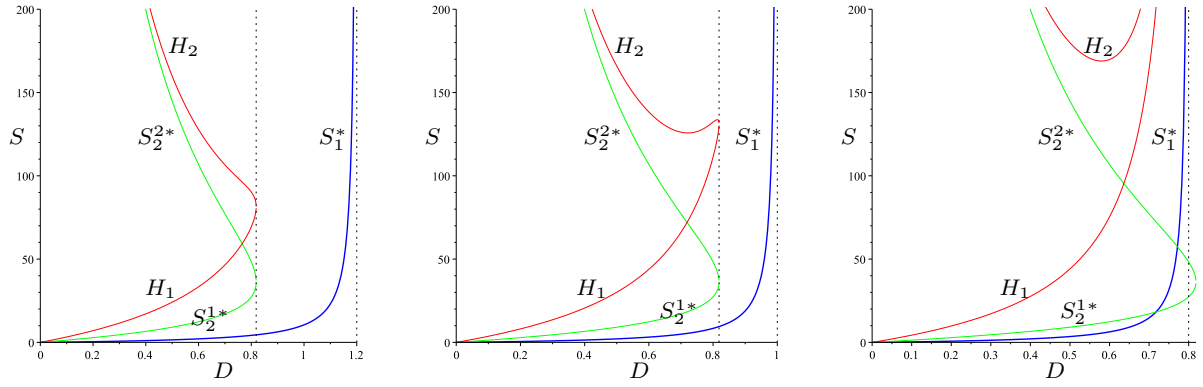

(a) $D_1 > D_2$, $dH_2/dD < 0$ (b) $D_1 > D_2$, H_2 non monotonous (c) $D_1 < D_2$

Fig. 1 The graphs of functions $S = S_1^*(D)$ (in Blue), $S = S_2^{i*}(D)$, $i = 1, 2$ (in Green) and $S = H_i(D)$, $i = 1, 2$ (in Red). (a): $m_1 = 0.6$; (b): $m_1 = 0.5$; (c): $m_1 = 0.4$. Other biological parameter values are given in Table 15. Compare with Fig. 4 of [25]

Table 6 Existence and stability of steady states of (2) in the nine regions of the operating space. GAS, S and U stand for *Globally asymptotically stable*, *Stable* (i.e. is Locally exponentially stable) and *Unstable* respectively. The last column shows the color in which the region is depiced in Figs. 2, 3, 4, 6, 7 and 8.

	E_1^0	E_1^1	E_1^2	E_2^0	E_2^1	E_2^2	Color
$\mathcal{I}_0$	GAS						Red
$\mathcal{I}_1$	U	GAS					Blue
$\mathcal{I}_2$	S	S	U				Cyan
$\mathcal{I}_3$	U			GAS			Yellow
$\mathcal{I}_4$	U			U	GAS		Green
$\mathcal{I}_5$	U			S	S	U	Pink
$\mathcal{I}_6$	U	U		U	GAS		Green
$\mathcal{I}_7$	U	U		S	S	U	Pink
$\mathcal{I}_8$	U	U	U	S	S	U	Pink

color in Table 6. Each color corresponds to different asymptotic behavior:

- *Red for the washout of both species, that is, the steady state E_1^0 is Globally asymptotically stable (GAS), which occurs in region $\mathcal{I}_0$.*
- *Blue for the washout of acidogenic bacteria while methanogenic bacteria are maintained, that is, the steady state E_1^1 is GAS, which occurs in region $\mathcal{I}_1$.*
- *Cyan for the bistability of E_1^0 and E_1^1 which are both (locally) stable. This behavior occurs in region $\mathcal{I}_2$. Depending on the initial condition the system, can go to the washout of both species or the washout of only the acidogenic bacteria.*
- *Yellow for the washout of methanogenic bacteria while acidogenic bacteria are maintained, that is the steady state E_2^0 is GAS, which occurs in region $\mathcal{I}_3$.*
- *Green for the global asymptotic stability of the positive steady state E_2^1, which occur in $\mathcal{I}_4$ and $\mathcal{I}_6$. These regions differ only by the existence, in the second region, of the unstable boundary steady state E_1^1.*
- *Pink for the bistability of E_2^0 and E_2^1 which are both locally asymptotically stable. This behavior occurs in regions $\mathcal{I}_5$, $\mathcal{I}_7$ and $\mathcal{I}_8$. These regions differ only by the possible existence of the unstable boundary steady states E_1^1 or E_1^2. Depending on the initial condition, the system can go to the washout of methanogenic bacteria or the coexistence of both species.*

It is worth noting that, from an experimental point of view, it is necessary to operate the bio-reactor in order to avoid the red region (E_1^0 is GAS) and the yellow region (E_2^0 is GAS). Green regions (E_2^1 is GAS) are the "target" operating regions, as they correspond to the global stability of the steady state, where all species survive, even if no addition of VFAs is provided ($S_{2\text{in}} = 0$ is permitted). Pink regions correspond to the bistability of E_2^0 (no biogas production) and E_2^1 (with biogas production). If the in-flowing concentration of the organic substrate ($S_{1\text{in}}$) is large enough, these regions necessarily appear. In these cases, for a good operation of the anaerobic digestion system, its state at start up should correspond to the convergence toward E_2^1 rather than E_2^0. The system can be operated in the blue and cyan region only if extraneous VFAs are added in the bio-reactor ($S_{2\text{in}} > 0$ is required).

The operating diagram highly depends on the shape of Γ_4 and Γ_5 surfaces, that is to say, on the behaviors of functions H_i, $i = 1, 2$, defined in Table 1. Notice that these functions are defined on $(0, \min(D_1, D_2))$ and H_1 is increasing, since it is the sum of two increasing functions. We have :

$$\lim_{D\to 0} H_1(D) = 0, \quad \lim_{D\to 0} H_2(D) = +\infty,$$

and

$$\lim_{D\to 0}\frac{dH_2}{dD}(D)=-\infty.$$

For the limits at right of the domain of definition of these functions, we must distinguish two cases:

– When $D_1 < D_2$, the functions H_i, $i = 1, 2$ are defined on $(0, D_1)$ and

$$\lim_{D\to D_1} H_1(D) = \lim_{D\to D_1} H_2(D) = +\infty.$$

– When $D_2 < D_1$, the functions H_i, $i = 1, 2$ are defined on $(0, D_2)$ and

$$\lim_{D\to D_2} H_1(D) = \lim_{D\to D_2} H_2(D) = S_2^M + \frac{k_2}{k_1}S_1^*(D_2),$$

$$\lim_{D\to D_2}\frac{dH_1}{dD}(D)=+\infty, \quad \lim_{D\to D_2}\frac{dH_2}{dD}(D)=-\infty.$$

Two qualitatively different sub-cases can be distinguished: either H_2 is decreasing on $(0, D_2)$ or it is not monotonous. Since H_2 is decreasing near the extremities of its definition interval, a typical example is where it is decreasing, then increasing and then decreasing.

Table 7 Three behaviors for functions H_i, $i = 1, 2$

Case (A), where $D_1 > D_2$ and $dH_2/dD < 0$.
Case (B), where $D_1 > D_2$ and H_2 non monotonous.
Case (C), where where $D_1 < D_2$.

Therefore there are three cases summarized in Table 7 and illustrated in Fig. 1. Since the surfaces Γ_i, $i = 1, \cdots, 6$, which are the boundaries of the various regions have been derived analytically, the operating diagrams can be drawn qualitatively in each of these cases. Instead of giving a general qualitative description of the operating diagram, and without loss of generality, we present the specific examples shown in Fig. 1. These examples are obtained with the Monod and Haldane functions 3. Notice that these functions satisfy Hypotheses 1 and 2. Therefore, the results of Propositions 1 and 2 apply. The analytical expressions of the auxiliary functions defined in Table 1 and needed in the defintions of the regions $\mathcal{I}_k$ of the operating diagrams are given in Table 12, in the particular case of functions 3. The biological parameter values used in the figures are given in Table 15. For the sake of practical applicability, these parameter values were chosen in a range that can be found in the literature [6,7]. Case (A) of Table 7, illustrated in Fig. 1(a), is obtained with the value $m_1 = 0.6$ of the maximum growth rate of acidogenic bacteria, while case (B) of Table 7, illustrated in Fig. 1(b), corresponds to $m_1 = 0.5$. Both values of m_1 are greater than the maximum growth rate $\mu_2(S_2^M)$ of methanogenic bacteria. These values are occurring in reality, because acidogenic reaction should be faster than the methanogenic one and, acidogenic bacteria are not be rapidly saturated compared with methanogenic bacteria. On the other hand, case (C) of Table 7, illustrated in Fig. 1(c), is obtained for $m_1 = 0.4$, which becomes slightly lower than $\mu_2(S_2^M)$. Although this case cannot be realistic, it is considered here to have a complete mathematical description of all possible scenarios. Moreover, it should be noted that the estimation of the kinetic parameters from experimental data have shown large values for the standard deviations, see Tables III and V in [7]. The values used in our simulations are in the limits given by the standard deviations.

For the biological parameter values corresponding to Fig. 1(a), the surfaces Γ_i, $i = 1, \cdots, 6$ are shown in Fig. 13. It is difficult to visualize the regions $\mathcal{I}_k$, $k = 0, \cdots, 8$ of the three-dimensional operating diagram. We can have a better understanding of these regions by showing cuts along 2 dimensional planes where one of the operating parameters is kept constant. For instance, if D is kept constant, we obtain then the operating diagram in the 2-dimensional plane $(S_{1\text{in}}, S_{2\text{in}})$. These operating diagrams are described in section 4. If $S_{2\text{in}}$ is kept constant, we obtain then the operating diagram in the 2-dimensional plane $(D, S_{1\text{in}})$. These operating diagrams are described in section 5.

4 Operating diagram in $(S_{1\text{in}}, S_{2\text{in}})$ where D is kept constant

The intersections of the surfaces Γ_i, $i = 1, \cdots, 5$ with a plane where D is kept constant are straight lines: vertical line for Γ_1, horizontal lines for Γ_2 and Γ_3 and oblique lines for Γ_4 and Γ_5, see Table 13. These straight lines separate the operating parameter plane $(S_{1\text{in}}, S_{2\text{in}})$ in up to nine regions $\mathcal{I}_k$, $k = 0, \cdots, 8$. Since the curves are straight lines, the regions of the operating diagram are very easy to picture. We begin by considering the case where $D_2 < D_1$ corresponding to Figs. 1(a) and 1(b).

4.1 Operating diagram when $D_2 < D_1$

The cuts at D constant of the 3-dimensional operating diagram shown in Fig. 13 and corresponding to Fig. 1(a), are shown in Fig. 2. The regions are colored according to the colors in Table 6. For the clarity of the picture all straight lines Γ_i are plotted in black. Fig. 2 shows the following features.

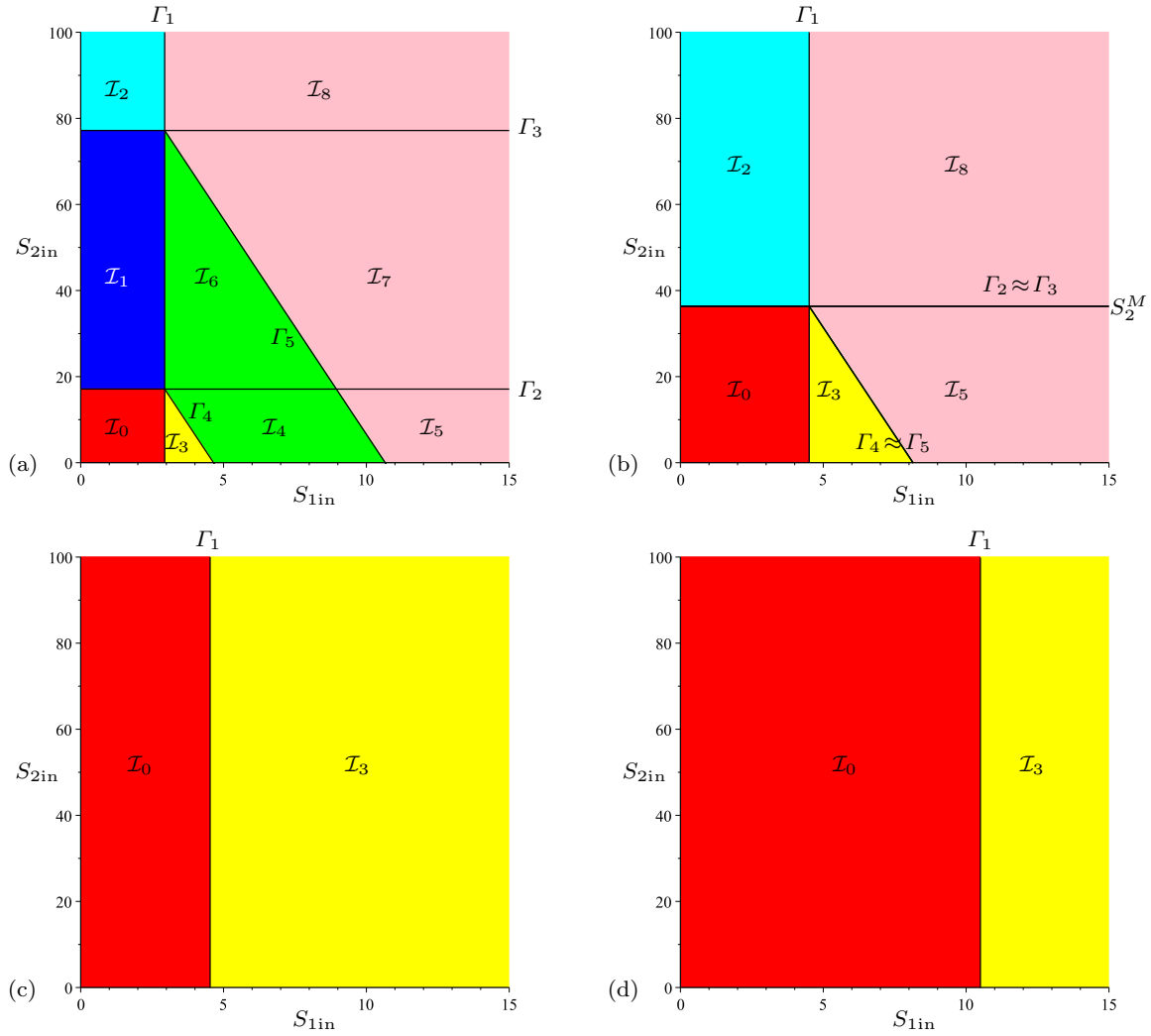

Fig. 2 The 2-dimensional operating diagram $(S_{1\mathrm{in}}, S_{2\mathrm{in}})$ obtained by cuts at D constant of the 3-dimensional operating diagram shown in Fig. 13. (a): $D = 0.7$; (b): $D = 0.818557 < D_2$; (c): $D = 0.82 > D_2$; (d): $D = 1 < D_1$. Here $D_1 = 1.2$, $D_2 \approx 0.818557467$ and $S_2^M \approx 36.332$.

For $0 < D < D_2$ all regions exist, see Fig. 2(a). For increasing D, the vertical line Γ_1 defined by $S_{1\mathrm{in}} = S_1^*(D)$ moves to the right and tends towards the vertical line defined by $S_{1\mathrm{in}} = S_1^*(D_2)$. At the same time, the horizontal lines Γ_2 and Γ_3, defined by $S_{2\mathrm{in}} = S_2^{1*}(D)$ and $S_{2\mathrm{in}} = S_2^{2*}(D)$, respectively, move towards each other and tend toward the horizontal line defined by $S_{2\mathrm{in}} = S_2^M$, so that the regions $\mathcal{I}_1$, $\mathcal{I}_4$, $\mathcal{I}_6$ and $\mathcal{I}_7$ shrink and disappear, see Fig. 2(b).

For $D = D_2$ the operating diagram changes dramatically, since regions $\mathcal{I}_1$, $\mathcal{I}_4$, $\mathcal{I}_6$, $\mathcal{I}_7$ shrink and disappear, see Fig. 2(b) obtained for $D = 0.818557 < D_2$, where $D_2 \approx 0.818557467$. At the same time regions $\mathcal{I}_0$, $\mathcal{I}_3$ invade the whole operating plane, so that regions $\mathcal{I}_2$, $\mathcal{I}_5$ and $\mathcal{I}_8$ also disappear, see Fig. 2(c) obtained for $D = 0.82 > D_2$.

For $D_2 < D < D_1$ only regions $\mathcal{I}_0$ and $\mathcal{I}_3$ appear, see Figs. 2(c) and 2(d). For increasing D, the vertical line Γ_1 defined by $S_{1\mathrm{in}} = S_1^*(D)$ moves to the right and tends towards infinity. For $D \geq D_1$ only region $\mathcal{I}_0$ appears.

The cuts D constant of the 3-dimensional operating diagram corresponding to Fig. 1(b), are shown in Fig. 3. This figure has the same qualitative characteristics as Fig. 2: presence of all regions when $0 < D < D_2$ as shown in Fig. 3(a); disappearance of all regions except regions $\mathcal{I}_0$ and $\mathcal{I}_3$, when $D = D_2$, as shown in the transition from Fig. 3(b) to Fig. 3(c); disappearance of region $\mathcal{I}_3$, when $D \geq D_1$, as shown in Fig. 3(d).

It is worth noting that the results shown in Figs. 2 and 3 are confirmatory of the expected behaviour in the anaerobic digestion process: Increasing D would expect to washout the species according to their existence conditions as a function of D. The methanogenic population cannot survive $D > D_2$, whereas the acidogenic does survive at higher dilution rates until $D \geq D_1$. Re-

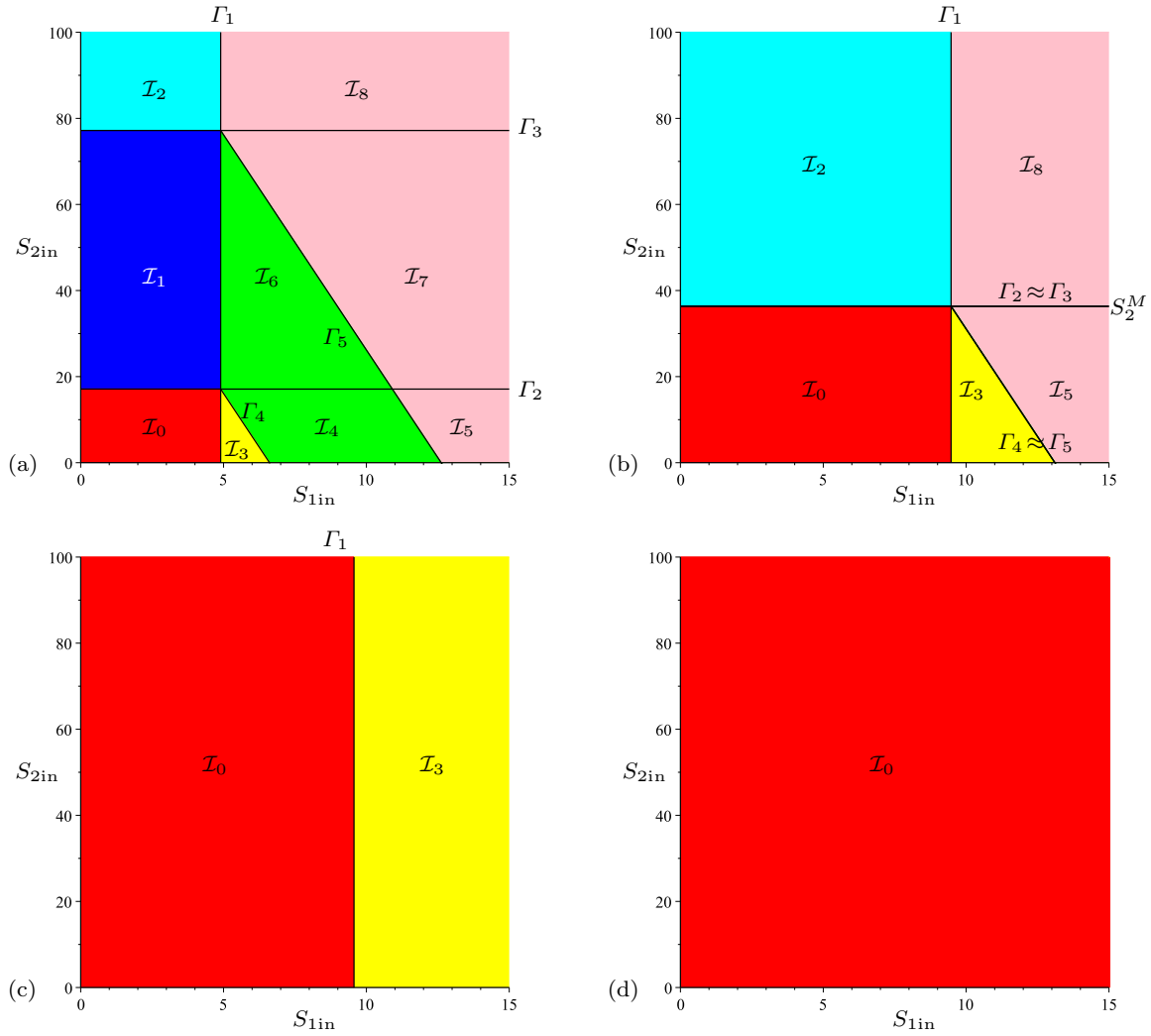

Fig. 3 The 2-dimensional operating diagram $(S_{1\text{in}}, S_{2\text{in}})$ with D constant, corresponding to Fig. 1(b). (a): $D = 0.7$; (b): $D = 0.818557 < D_2$; (c): $D = 0.82 > D_2$; (d): $D = 1 \geq D_1$. Here $D_1 = 1$, $D_2 \approx 0.818557467$ and $S_2^M \approx 36.332$.

ducing the acidogenic bacteria growth rate results in washout of the acidogenic population at lower dilution rates: $D_1 = 1.2$ in Fig. 2, where $m_1 = 0.6$, while $D_1 = 1$ in Fig. 3, where $m_1 = 0.5$.

4.2 Operating diagram when $D_1 < D_2$

The cuts D constant of the 3-dimensional operating corresponding to Fig. 1(c), are shown in Fig. 4. The regions are colored according to the colors in Table 6. Fig. 4 shows the following features.

For $0 < D < D_1$ all regions appear, see Fig. 4(a). For increasing D, the vertical line Γ_1 defined by $S_{1\text{in}} = S_1^*(D)$ moves to the right and tends towards infinity. At the same time, the horizontal lines Γ_2 and Γ_3, defined by $S_{2\text{in}} = S_2^{1*}(D)$ and $S_{2\text{in}} = S_2^{2*}(D)$, respectively, move towards each other, as depicted in Fig. 4(b), and tend towards the horizontal lines defined by $S_{2\text{in}} = S_2^{1*}(D_1)$ and $S_{2\text{in}} = S_2^{2*}(D_1)$, respectively, as depicted in Fig. 4(c).

For $D = D_1$, the operating diagram changes dramatically: all regions $\mathcal{I}_3$, $\mathcal{I}_4$ and $\mathcal{I}_5$, $\mathcal{I}_6$, $\mathcal{I}_7$ and $\mathcal{I}_8$ have disappeared since they are located to the right of the vertical Γ_1 which tends toward infinity, when D tends to D_1, as depicted in Fig. 4(c).

For $D_1 \leq D < D_2$ only regions $\mathcal{I}_0$, $\mathcal{I}_1$, and $\mathcal{I}_2$ appear. For increasing D, the horizontal lines Γ_2 and Γ_3, defined by $S_{2\text{in}} = S_2^{1*}(D)$ and $S_{2\text{in}} = S_2^{2*}(D)$, respectively, move towards each other and tend toward the horizontal line defined by $S_{2\text{in}} = S_2^M$, so that region $\mathcal{I}_1$ shrinks, as $D \to D_2$, and disappears when $D = D_2$, see Fig. 4(d). For $D > D_2$, the region $\mathcal{I}_0$ invades the whole operating plane, as in Fig. 3(d).

It is worth noting that the results shown in Fig. 4 show now an unexpected behavior for the anaerobic digestion process: increasing D, we now have the phe-

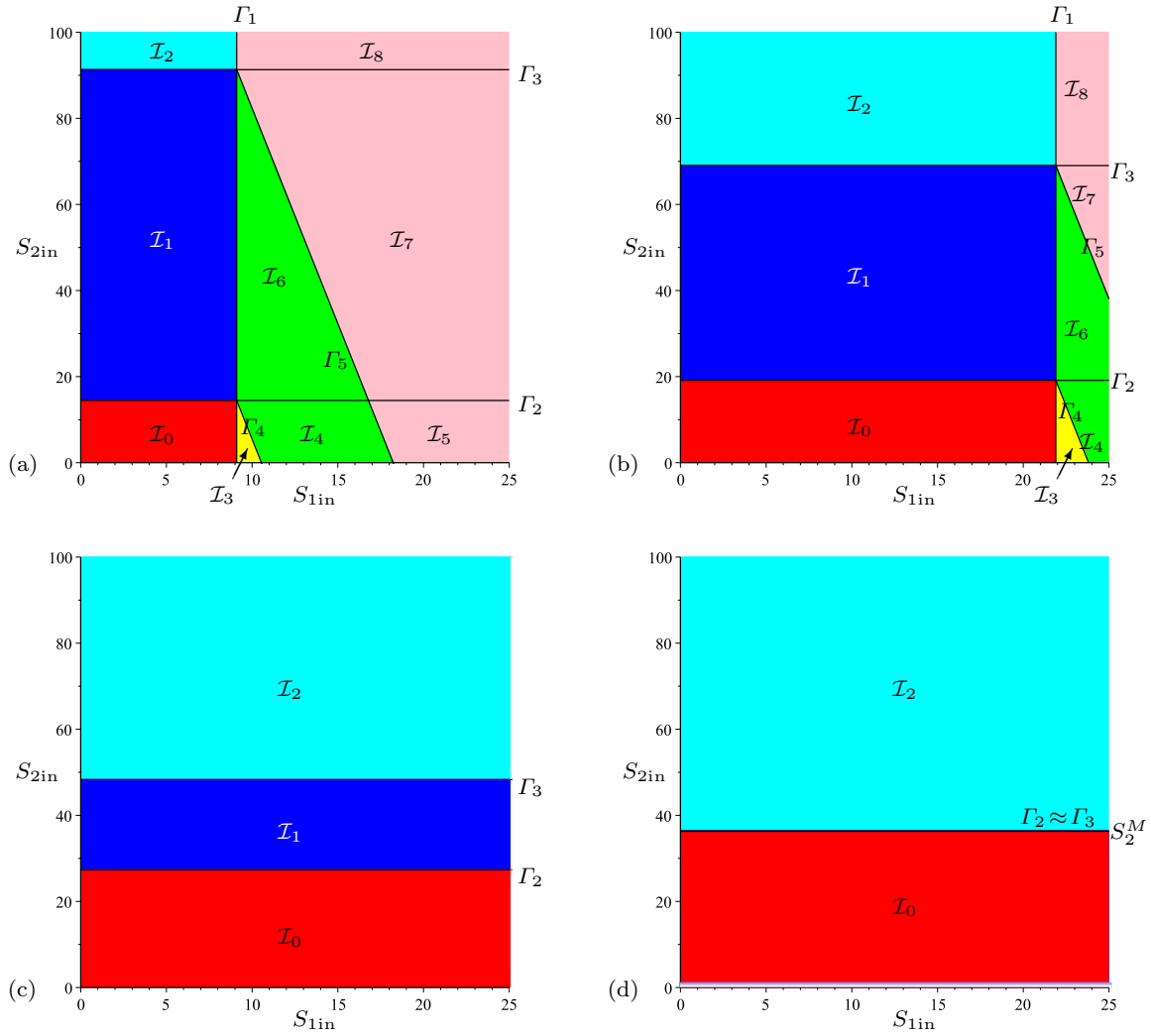

Fig. 4 The 2-dimensional operating diagram $(S_{1\text{in}}, S_{2\text{in}})$ with D constant, corresponding to Fig. 1(c). (a): $D = 0.65$; (b): $D = 0.73$; (c): $D = D1 = 0.8$; (d): $D = 0.818557 < D_2$. Here $D_2 \approx 0.818557467$ and $S_M^2 \approx 36.332$.

nomenon where the acidogenic population washout first, but this is unrealistic in practice. As mentioned before, we consider this important case from mathematical point of view, in order to deeply analyze the operating diagrams for a generic two-step system, and to show its predictions from the technological point of view. It it is possible that for another two-step system, the kinetic parameters are such that the second population X_2 will washout first.

The results shown in Fig. 2, 3 and 4 are confirmatory of another expected behaviour of the anaerobic digestion process. It is seen in these operating diagrams that when $D < \min(D_1, D_2)$ is kept constant, and $S_{1\text{in}}$ increases, there is a loss of GAS, since the system goes from the Green region to the Pink region. This behavior also occurs as $S_{2\text{in}}$ increases and $S_{1\text{in}} > S_1^*(D)$ is kept constant, i.e. by increasing the supply of extraneous substrates, we allow for bistability, essentially moving from unstable (in the green region) to stable (in the pink region) steady state E_2^0.

5 Operating diagram in $(D, S_{1\text{in}})$ where $S_{2\text{in}}$ is kept constant

The intersections of Γ_2 and Γ_3 and Γ_6 surfaces with a plane where $S_{2\text{in}}$ is kept constant are vertical lines, and the intersections of Γ_1, Γ_4 and Γ_5 surface with this plane are curves of functions of D, as shown in Table 14. Curves Γ_1 and Γ_6 do not depend on $S_{2\text{in}}$ while curves Γ_2, Γ_3, Γ_4 and Γ_5 depend on $S_{2\text{in}}$. Note that curves Γ_4 and Γ_5 simply consist of translating downwards the H_1 and H_2 function curves, shown in Fig. 1, and multiplying by k_1/k_2. For details on how to plot these curves, the reader is referred to Appendix C. The curves Γ_k, $k = 1, \cdots, 6$, separate the operating parameter plane $(D, S_{1\text{in}})$ in up to nine regions $\mathcal{I}_k$, $k = 0, \cdots, 8$. We

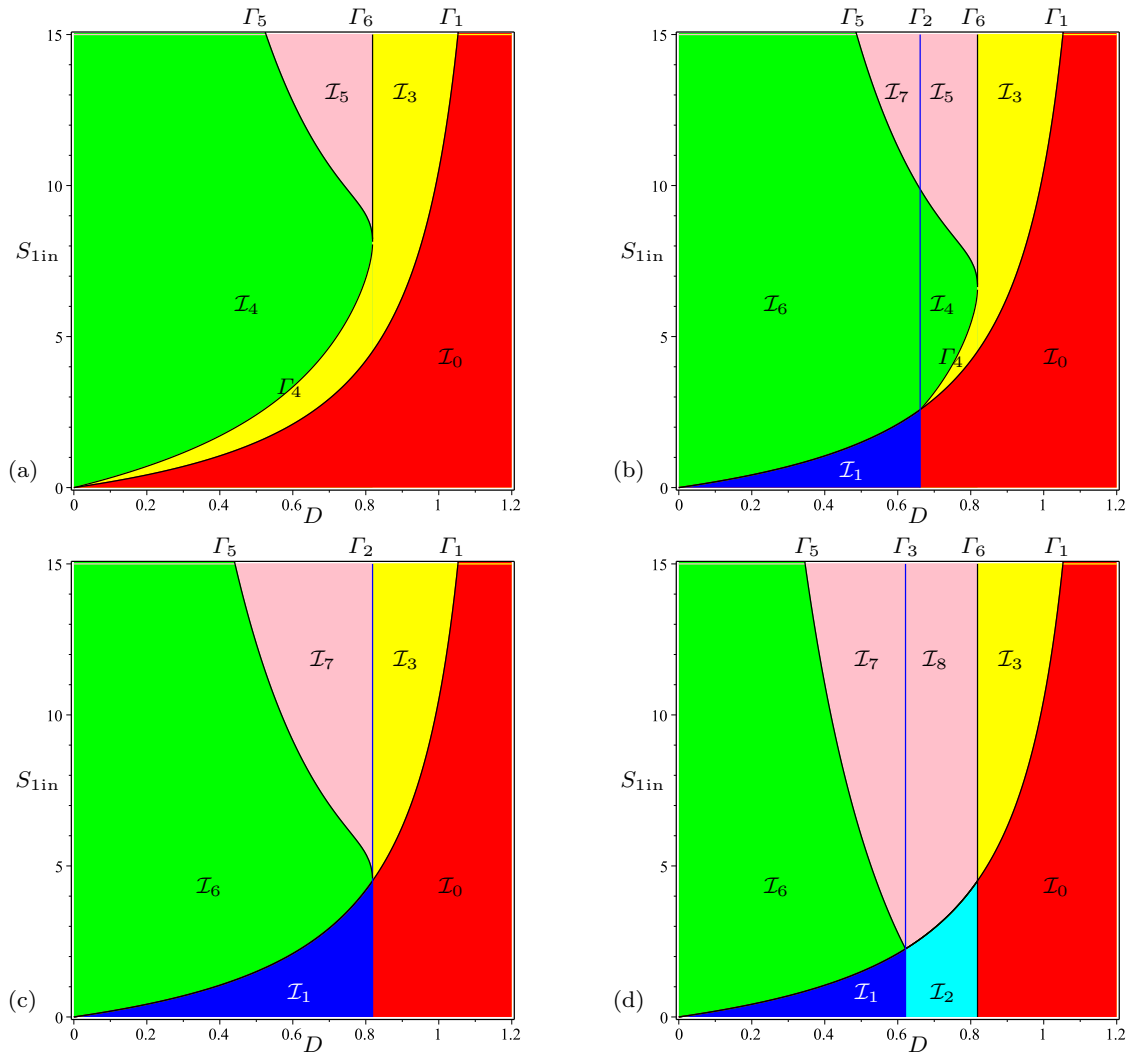

Fig. 5 The 2-dimensional operating diagram (D, S_{1in}) obtained by cuts at S_{2in} constant of the 3-dimensional operating diagram shown in Fig. 13 and corresponding to Fig. 1(a). (a): $S_{2in} = 0$, (b): $S_{2in} = 15$, (c): $S_{2in} = S_2^M \simeq 36.332$ and (d): $S_{2in} = 100$.

begin by considering the case where $D_2 < D_1$ corresponding to Figs. 1(a) and 1(b).

5.1 Operating diagram when $D_2 < D_1$

The cuts at S_{2in} constant of the 3-dimensional operating diagram shown in Fig. 13 and corresponding to Fig. 1(a), are shown in Fig. 5. The regions are colored according to the colors in Table 6. Fig. 5 shows the following features.

For $S_{2in} = 0$, only the regions $\mathcal{I}_0, \mathcal{I}_3, \mathcal{I}_4$ and $\mathcal{I}_5$ exist, see Fig. 5(a). For $0 < S_{2in} < S_2^M$, Γ_2 curve appears, giving birth to $\mathcal{I}_1$, $\mathcal{I}_6$ and $\mathcal{I}_7$ regions, see Fig. 5(b). For increasing S_{2in}, Γ_4 and Γ_5 curves are translated downwards, while the vertical line Γ_2 moves to the right and tends towards the vertical line Γ_6, as S_{2in} tends to S_2^M.

For $S_{2in} = S_2^M$, Γ_4 curve disappears, while Γ_2 becomes equal to Γ_6, so that $\mathcal{I}_4$ and $\mathcal{I}_5$ regions have disappeared, see Fig. 5(c). For $S_{2in} > S_2^M$, Γ_3 curve appears, giving birth to $\mathcal{I}_2$ and $\mathcal{I}_8$ regions, see Fig. 5(d). For increasing S_{2in}, the vertical line Γ_3 moves to the left, while Γ_5 curve is translated downwards.

The cuts S_{2in} constant of the 3-dimensional operating diagram corresponding to Fig. 1(b), are shown in Fig. 6. This figure has the same qualitative characteristics as Fig. 5: presence of only $\mathcal{I}_0$, $\mathcal{I}_3$, $\mathcal{I}_4$ and $\mathcal{I}_5$ regions when $S_{2in} = 0$, see Fig. 6(a); appearance of $\mathcal{I}_1$, $\mathcal{I}_6$ and $\mathcal{I}_7$ regions when $0 < S_{2in} < S_2^M$, see Fig. 6(b); disappearance of $\mathcal{I}_4$ and $\mathcal{I}_5$ regions when $S_{2in} = S_2^M$, see Fig. 6(c); appearance of $\mathcal{I}_2$ and $\mathcal{I}_8$ regions when $S_{2in} > S_2^M$, see Fig. 6(d).

It is worth noting that the results shown in Figs. 5 and 6 are confirmatory of the expected behaviour in the

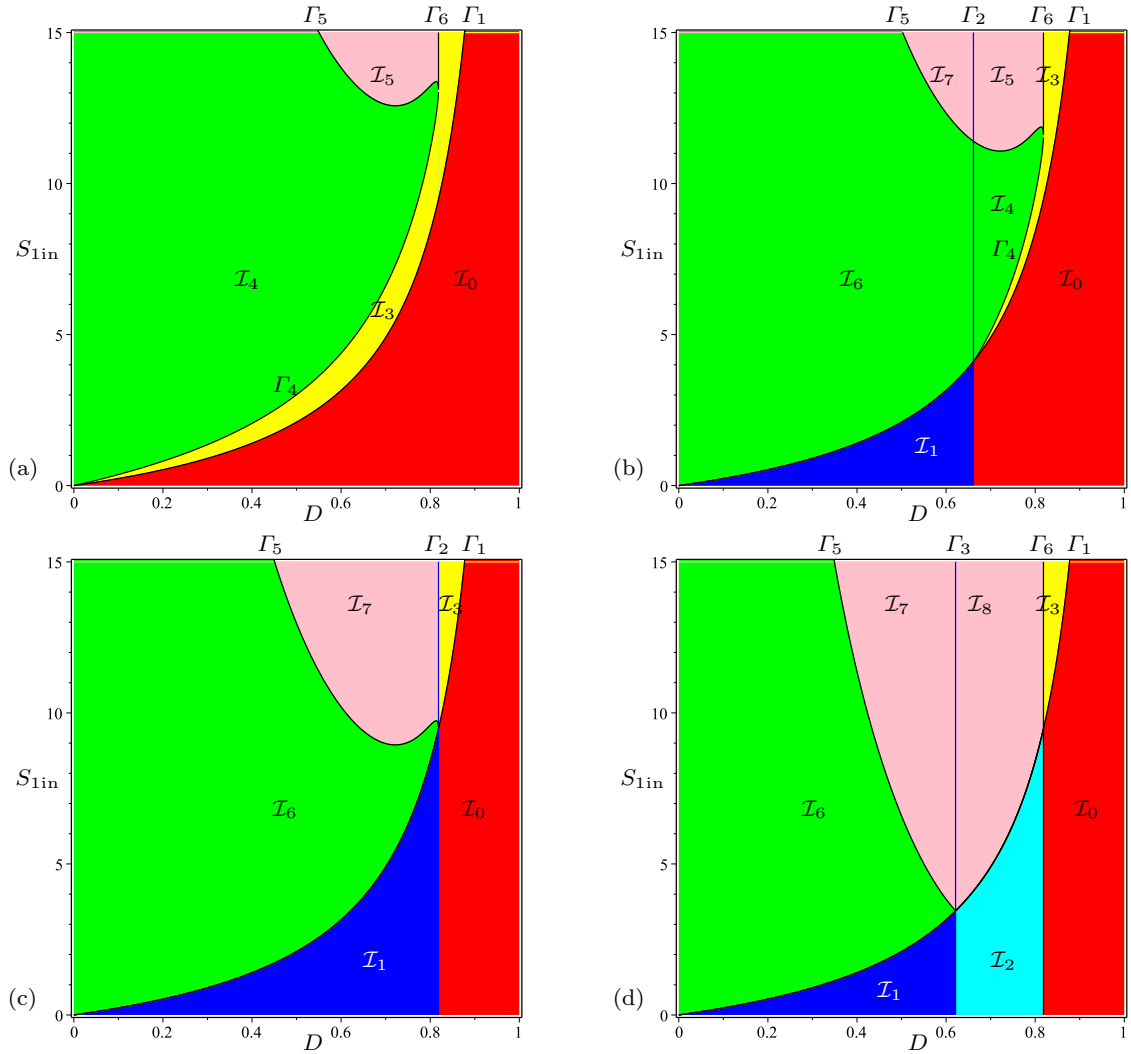

Fig. 6 The 2-dimensional operating diagram $(D, S_{1\text{in}})$ obtained by cuts at $S_{2\text{in}}$ constant of the 3-dimensional operating diagram corresponding to Fig. 1(b). (a): $S_{2\text{in}} = 0$, (b): $S_{2\text{in}} = 15$, (c): $S_{2\text{in}} = S_2^M \approx 36.332$ and (d): $S_{2\text{in}} = 100$.

anaerobic digestion process. First, the addition of extraneous VFAs is not required in the system: Figs. 5(a) and 6(a) show that even with $S_{2\text{in}} = 0$, the bio-reactor can be properly operated. Second, decreasing D would expect to stabilize the system. For instance, if for any reason, the system is operated in the red region (washout out of all species) or yellow region (washout of the methanogenic bacteria) we need only to reduce the dilution rate, to attain the Pink, Blue or Green region, where the methanogenic bacteria are maintained. Indeed, decreasing D allows a higher retention time for bacteria to growth into the bio-reactor. Moreover, lowering the dilution rate leads from the bistability Pink region to the Green region of global stability of the steady state stability, where both populations are maintained. However, in Fig. 6, the model presents the very surprising property where the bio-reactor can go from the bistability region (the pink region $\mathcal{I}_5$ or $\mathcal{I}_7$), to global asymptotic stability of the positive steady state E_2^1 (the green regions $\mathcal{I}_4$ or $\mathcal{I}_6$), when the dilution rate D increases. Indeed, the common boundary Γ_5 of Green and Pink regions has an increasing part, with respect to parameter D. Therefore, near this part of Γ_5, as $S_{1\text{in}}$ and $S_{2\text{in}}$ are kept constant and D increases the system goes from $\mathcal{I}_5$ to $\mathcal{I}_4$, see Fig. 6(a) and 6(b), or goes from $\mathcal{I}_7$ to $\mathcal{I}_6$, see Fig. 6(c).

This possibility of globally stabilizing the system, which presents bistability, is surprising since the global stability of the positive steady state is more likely obtained by decreasing D rather than increasing it. This unespecated behavior was first observed in a slightly different two-step model, where the first kinetics is of Contois type [13].

It is worth-noting that this unexpected behavior can occur only for suitable values of the biological parameters. For instance, in Fig. 5, where all biological pa-

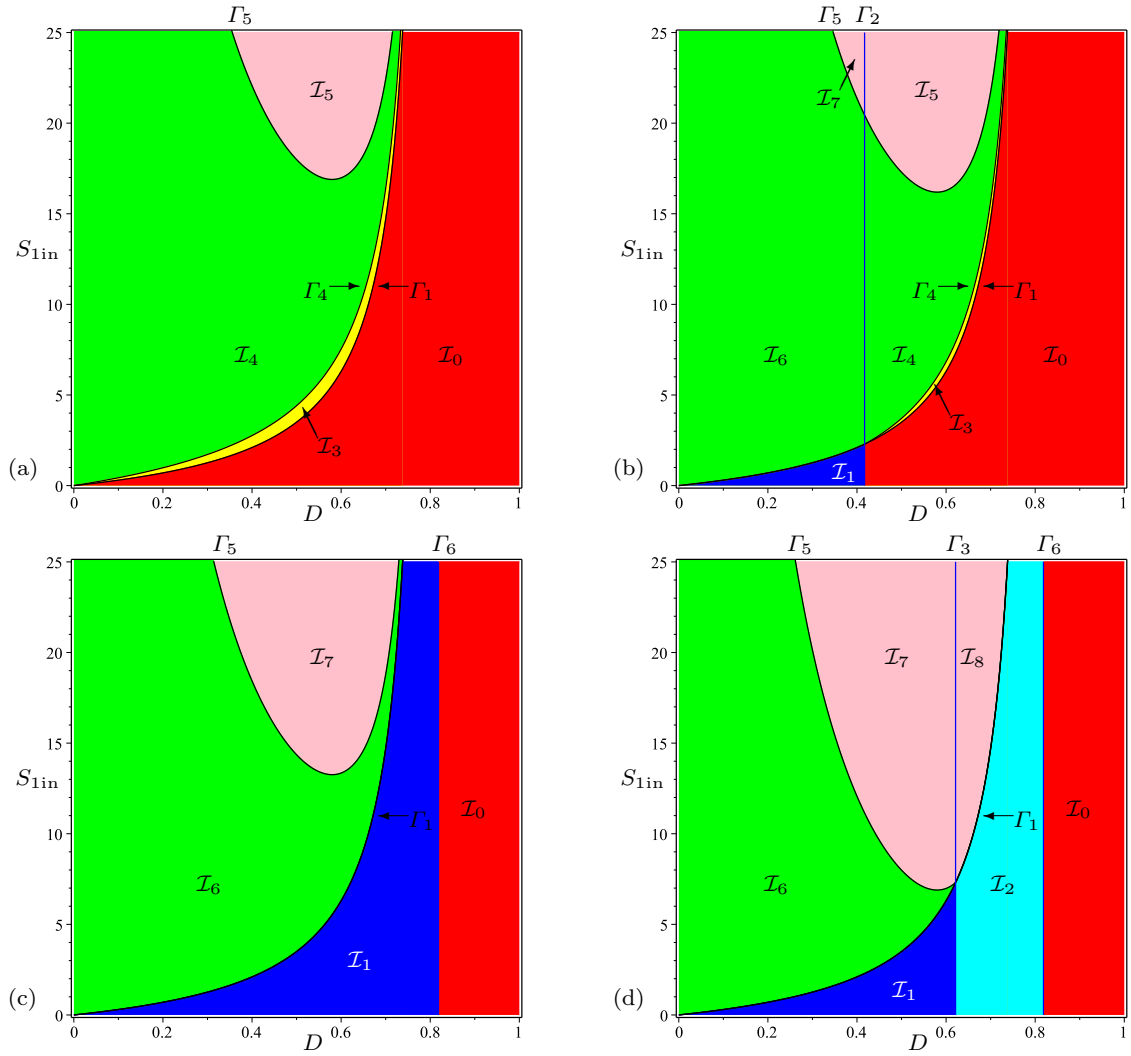

Fig. 7 The 2-dimensional operating diagram $(D, S_{1\mathrm{in}})$ obtained by cuts at $S_{2\mathrm{in}}$ constant of the 3-dimensional operating diagram corresponding to Fig. 1(c). (a): $S_{2\mathrm{in}} = 0$, (b): $S_{2\mathrm{in}} = 7$, (c): $S_{2\mathrm{in}} = S_2^M \simeq 36.3$ and (d): $S_{2\mathrm{in}} = 100$.

rameters are the same as in Fig. 6, excepted that m_1 is changed from $m_1 = 0.5$ to $m_1 = 0.6$, the behavior does not occur and a transition from Pink region to Green region is possible only by decreasing D.

5.2 Operating diagram when $D_1 < D_2$

The cuts at $S_{2\mathrm{in}}$ constant of the 3-dimensional operating diagram corresponding to Fig. 1(c), are shown in Fig. 7. The regions are colored according to the colors in Table 6. Since $D_1 < D_2$ there exists a value $S_2^0 < S_2^M$ such that $\mu_2(S_2^0) = \alpha D_1$.

Fig. 7 shows the following features. For $S_{2\mathrm{in}} = 0$, only regions $\mathcal{I}_0, \mathcal{I}_3, \mathcal{I}_4$ and $\mathcal{I}_5$ appear, see Fig. 7(a). For $0 < S_{2\mathrm{in}} < S_2^0$, Γ_2 curve appears, giving birth to $\mathcal{I}_1, \mathcal{I}_6, \mathcal{I}_7$ regions, see Fig. 7(b). For increasing $S_{2\mathrm{in}}$, Γ_4 and Γ_5 curves are translated downwards, while the vertical line Γ_2 moves to the right and tends towards the common vertical asymptote $D = D_1$ for curves Γ_1, Γ_4 and Γ_5, as $S_{2\mathrm{in}}$ tends to S_2^0. In the limit $S_{2\mathrm{in}} = S_2^0$, the very tiny region $\mathcal{I}_3$ (in Yellow on the figure) located between curves Γ_1 and Γ_4, together with $\mathcal{I}_4$ and $\mathcal{I}_5$ regions have disappeared.

For $S_2^0 < S_{2\mathrm{in}} \leq S_2^M$, only regions $\mathcal{I}_0, \mathcal{I}_1, \mathcal{I}_6$ and $\mathcal{I}_7$ exist. For increasing $S_{2\mathrm{in}}$, the vertical line Γ_2 moves to the right and tends towards Γ_6 as $S_{2\mathrm{in}}$ tends to S_2^M, see Fig. 7(c). For $S_{2\mathrm{in}} > S_2^M$, Γ_3 curve appears, giving birth to $\mathcal{I}_2$ and $\mathcal{I}_8$ regions, see Fig. 7(d). For increasing $S_{2\mathrm{in}}$, the vertical line Γ_3 moves to the left while Γ_5 curve is translated downwards.

It should be noticed that as in Fig. 6, it is seen in Fig. 7 that the region of global asymptotic stability of the positive steady state E_2^1 (the Green region $\mathcal{I}_4 \cup \mathcal{I}_6$) presents the property that there exists a range of values for the operating parameters $S_{1\mathrm{in}}$ and $S_{2\mathrm{in}}$ such that the system can go from the bistability region (the

Table 8 Codimension-one bifurcations along subsets of surfaces Γ_k and the corresponding cases in [6]: Transcritical bifurcations (TB) and Saddle Node bifurcations (SNB) occur.

Γ_k	Subset of Γ_k	Bifurcation	Case of [6]
Γ_1	$\Gamma_1 \cap \{0 \leq S_{2\text{in}} < S_2^{1*}(D)\}$	TB: $E_1^0 = E_2^0$	
	$\Gamma_1 \cap \{S_2^{1*}(D) < S_{2\text{in}} < S_2^{2*}(D)\}$	TB: $E_1^i = E_2^i$, $i = 0, 1$	
	$\Gamma_1 \cap \{S_{2\text{in}} > S_2^{2*}(D)\}$	TB: $E_1^i = E_2^i$, $i = 0, 1, 2$	
Γ_2	Γ_2	TB: $E_1^0 = E_1^1$	**1.4**, **2.8**, **2.9**
Γ_3	Γ_3	TB: $E_1^0 = E_1^2$	**1.5**, **2.13**
Γ_4	Γ_4	TB: $E_2^0 = E_2^1$	**2.7**
Γ_5	Γ_5	TB: $E_2^0 = E_2^2$	**2.12**, **2.15**
Γ_6 $D_2 < D_1$	$\Gamma_6 \cap \left\{0 \leq S_{2\text{in}} < S_2^M \text{ and } S_{1\text{in}} > S_1^*(D_2) + \frac{k_1}{k_2}\left(S_2^M - S_{2\text{in}}\right)\right\}$	SNB: $E_2^1 = E_2^2$	**2.11**
	$\Gamma_6 \cap \left\{S_{2\text{in}} > S_2^M \text{ and } S_{1\text{in}} > S_1^*(D_2)\right\}$	SNB: $E_j^1 = E_j^2$, $j = 1, 2$	**2.14**
	$\Gamma_6 \cap \left\{S_{2\text{in}} > S_2^M \text{ and } S_{1\text{in}} < S_1^*(D_2)\right\}$	SNB: $E_1^1 = E_1^2$	**1.6**
Γ_6 $D_1 < D_2$	$\Gamma_6 \cap \left\{S_{2\text{in}} > S_2^M \text{ and } S_{1\text{in}} > 0\right\}$	SNB: $E_1^1 = E_1^2$	**1.6**

Pink region $\mathcal{I}_5 \cup \mathcal{I}_7$), to the global asymptotic stability region, when the dilution rate D increases. This behavior, obtained in the case $D_2 > D_1$, was investigated in [15]. Our findings show that this unexpected scenario, where increasing the dilution rate can globally stabilize two-step biological systems can occur also in the rather more realistic case $D_2 < D_1$, depicted in Fig. 6, and not only in the less realistic case $D_2 > D_1$ studied in [15].

It is worth noting that the results shown in Figs. 5, 6 and 7 are confirmatory of the expected behaviour in the anaerobic digestion process. As was depicted also in Figs. 2, 3 and 4, it is seen that when $D < \min(D_1, D_2)$ is kept constant, and $S_{1\text{in}}$ increases, there is a loss of GAS, since the system goes from the Green region to the Pink region.

6 Bifurcations

The surfaces Γ_k, $k = 1, \cdots, 6$, are the borders of the regions in the operating parameters space $(D, S_{1\text{in}}, S_{2\text{in}})$ on which bifurcations occur, while the steady states change their stability. In codimension-one bifurcations, only transcritical and saddle node bifurcations can be encountered, as stated in the following result.

Proposition 3 *The bifurcations of the steady states of (2) arising on the boundaries of regions $\mathcal{I}_k$, $k = 0, \cdots, 8$, are listed in Table 8.*

Proof The proof is given in Appendix B.3. □

Remark 2 *The last column of Table 8 shows the corresponding cases with* non hyperbolic *steady states given in Theorem 1 of [6]. The case labeled* **2.10** *in this theorem, where $E_1^0 = E_1^1$ and $E_2^0 = E_2^2$, does not appear in Table 8, since it is a codimension-two bifurcation arising along $\Gamma_2 \cap \Gamma_5$. The bifurcations along Γ_1, corresponding to the condition $S_{1\text{in}} = S_1^*(D)$ were not analyzed in [6]. In Theorem 1 of [6] only the cases $S_{1\text{in}} < S_1^*(D)$ and $S_{1\text{in}} > S_1^*(D)$ were considered.*

To have a better understanding of the nature of the bifurcations of steady states, let us consider the dilution rate D as the bifurcation parameter. Throughout this section, we assume that biological parameters are fixed as in Fig. 6(a), corresponding to case (b) of Fig. 1 and $S_{2\text{in}} = 0$. We now fix the operating parameter $S_{1\text{in}}$ at various typical values, as depicted in the horizontal lines shown in Fig. 8, and plot one-parameter bifurcation diagrams in D, with X_i, $i = 1, 2$, on the y-axis, see Fig. 9, 10 and 11.

Recall that the curve Γ_5 separating the Pink and Green regions is the curve of the function $S_{1\text{in}} = \frac{k_1}{k_2} H_2(D)$. Case (B) corresponds to a function H_2 which is decreasing, then increasing, then decreasing. For the considered biological parameters values, the function $H_2(D)$ attains its minimum for $D_{min} \simeq 0.72$ and its maximum for $D_{max} = 0.81$ and satisfies $H_2(D_2) = S_2^M + \frac{k_2}{k_1} S_1^*(D_2) \simeq 131.1$, where $D_2 = \frac{1}{\alpha}\mu_2\left(S_2^M\right) \simeq 0.82$. Therefore, the variations of $\frac{k_1}{k_2} H_2(D)$ are as shown in the following table

D	0		0.72		0.81		0.82
$\frac{k_1}{k_2} H_2(D)$	$+\infty$	$\searrow$	12.57	$\nearrow$	13.37	$\searrow$	13.11

We fix three typical values $S_{1\text{in}} = 13$, $S_{1\text{in}} = 13.3$ and $S_{1\text{in}} = 14$, corresponding to the three horizontal lines shown in Fig. 8. The corresponding bifurcation values D_k, $k = 2, \cdots, 10$, of D are defined in Table 9.

We begin with the case where $S_{1\text{in}} = 14$. Since $S_{1\text{in}} > 13.37$, as it is seen in Fig. 8, with increasing D, there is a transition from $\mathcal{I}_4$ to $\mathcal{I}_5$ for $D = D_5$, then from $\mathcal{I}_5$ to $\mathcal{I}_3$ for $D = D_2$, then from $\mathcal{I}_3$ to $\mathcal{I}_0$

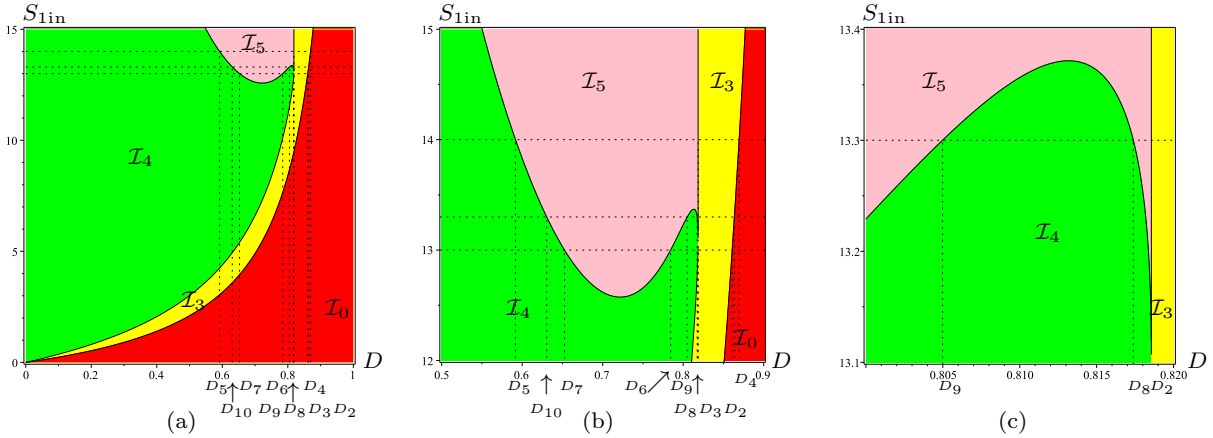

Fig. 8 Operating diagram where $S_{2in} = 0$ corresponding to Fig. 6(a). (a): Cuts where S_{1in} is kept constant and D is the bifurcation parameter. (b): Magnification of the operating diagram showing the bifurcation values D_k, defined in Table 9. Notice that there are three different values of D_4 corresponding to the three different values $S_{1in} = 13$, $S_{1in} = 13.3$ and $S_{1in} = 14$. (c) : Magnification showing the values $D = D_9$, $D = D_8$ and $D = D_2$.

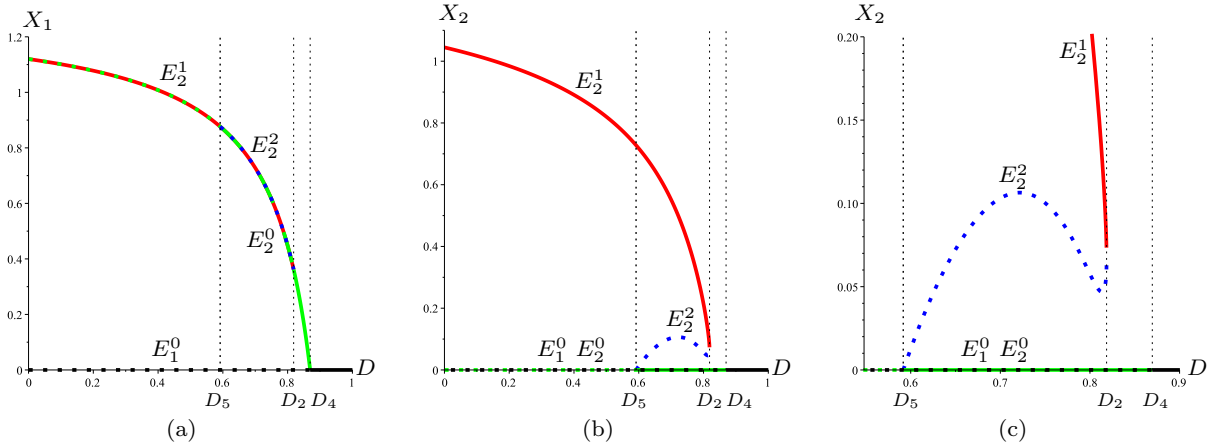

Fig. 9 Bifurcation diagram with D as the bifurcation parameter, corresponding to Fig. 6(a) and $S_{1in} = 14$. (a): The X_1-components and (b): the X_2-components, of the steady states E_1^0 (in Black), E_2^0 (in Green), E_2^1 (in Red) and E_2^2 (in Blue). (c): A magnification showing the bifurcation values D_2, D_4 and D_5. Solid lines and dotted lines correspond to stable and unstable steady states respectively.

Table 9 The bifurcation values D_k, $k = 2, \cdots, 10$, corresponding to $S_{2in} = 0$ and $S_{1in} = 13$, $S_{1in} = 13.3$ or $S_{1in} = 14$.

S_{1in}	$D_2 = \frac{\mu_2(S_2^M)}{\alpha}$	$D_4 = \frac{\mu_1(S_{1in})}{\alpha}$	D_3 is the solution of $S_{1in} = \frac{k_1}{k_2} H_1(D)$	D_k, $k = 5, \cdots, 10$ are the solutions of $S_{1in} = \frac{k_1}{k_2} H_2(D)$
14	$D_2 \approx 0.8186$	$D_4 \approx 0.8696$		$D_5 \approx 0.5917$
13		$D_4 \approx 0.8609$	$D_3 \approx 0.8184$	$D_6 \approx 0.7844$, $D_7 \approx 0.6526$
13.3	$D_2 \approx 0.8186$	$D_4 \approx 0.8636$		$D_8 \approx 0.8173$, $D_9 \approx 0.8050$, $D_{10} \approx 0.6304$

for $D = D_4$. The bifurcation values D_2, D_4 and D_5 are given in Table 9. The bifurcation value D_4 corresponds to a transcritical bifurcation of E_2^0 and E_1^0; D_2 corresponds to a saddle node bifurcation of E_2^1 and E_2^2 and D_5 corresponds to a transcritical bifurcation of E_2^0 and E_2^2. The plot of X_1 and X_2 components of all existing steady states with respect of D is shown in Fig. 9. Solid lines and dotted lines correspond to stable and unstable steady states respectively. Since $S_{2in} = 0$, the steady states E_1^1 and E_1^2 cannot exist. On Fig. 9(a), for $0 < D < D_5$, the X_1-component of E_2^i, $i = 0, 2$, is colored in Red, with Green dots, showing the stability of E_2^1 and the instability of E_2^0. For $D_5 < D < D_2$, the X_1-component of E_2^i, $i = 0, 1, 2$, is colored in Red and Green, with Blue dots, showing the bistability of E_2^0 and E_2^1 and the instability of E_2^1. For $D_2 < D < D_4$, the X_1-component of E_2^0 is colored in Green, showing the stability of E_2^0. On Fig. 9(b) and 9(c), for $0 < D < D_2$,

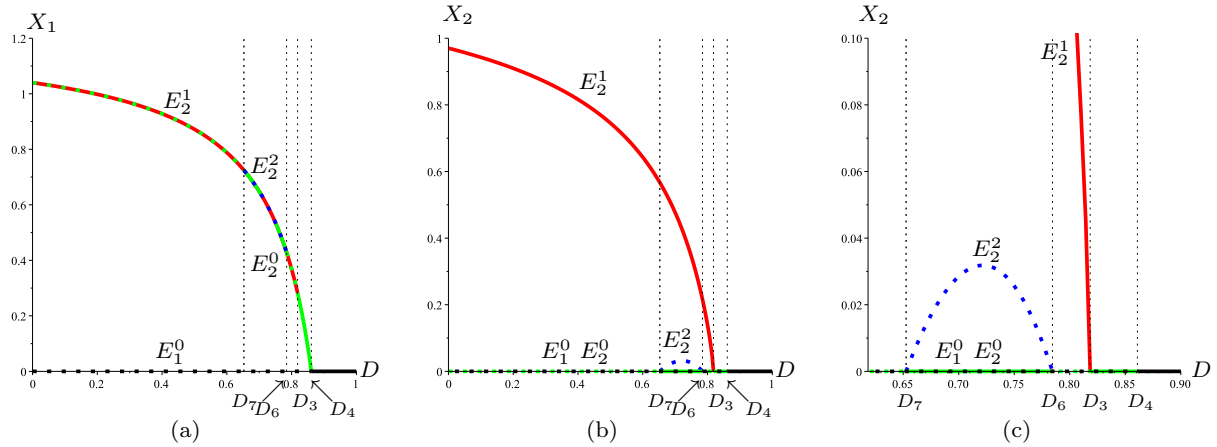

Fig. 10 Bifurcation diagram with D as the bifurcation parameter, corresponding to Fig. 6(a) and $S_{1\text{in}} = 13$. (a): The X_1-components and (b): the X_2-components, of the steady states E_1^0 (in Black), E_2^0 (in Green), E_2^1 (in Red) and E_2^2 (in Blue). (c): A magnification showing the bifurcation values D_3, D_4, D_6 and D_7. Solid lines and dotted lines correspond to stable and unstable steady states respectively.

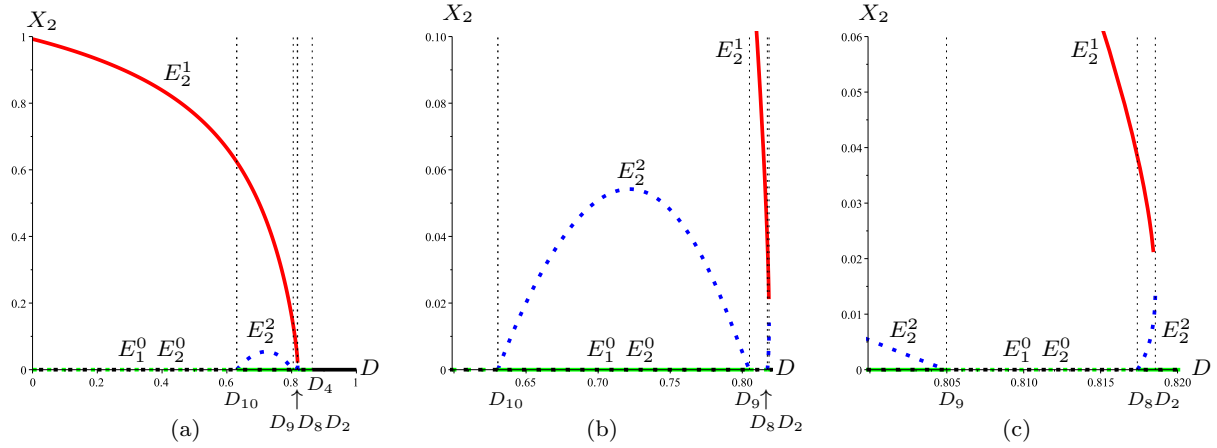

Fig. 11 Bifurcation diagram with D as the bifurcation parameter, corresponding to Fig. 6(a) and $S_{1\text{in}} = 13.3$. (a): The X_2-components of the steady states E_1^0 (in Black), E_2^0 (in Green), E_2^1 (in Red) and E_2^2 (in Blue). (b): A magnification showing the bifurcation values D_9 and D_{10}, where D_2 and D_8 are indistinguishable. (c): A larger magnification showing the bifurcation values D_2, D_8 and D_9. Solid lines and dotted lines correspond to stable and unstable steady states respectively.

the $X_2 = 0$-component of E_j^0, $j = 1, 2$, is colored with Green and Black dots, showing the instability of E_2^0 and E_1^0. For $D_2 < D < D_4$ it is colored in Green, with Black dots, showing the stability of E_2^0 and the instability of E_1^0. For $D > D_4$ it is colored in Black showing the stability of E_1^0.

Consider now the case where $S_{1\text{in}} = 13$. This case corresponds to the surprising situation where we can go from the bistability region (colored in Pink) to the global asymptotic stability region (colored in Green), when the dilution rate D increases. Since $12.57 < S_{1\text{in}} < 13.11$, as it is seen in Fig. 8, with increasing D, there is a transition from $\mathcal{I}_4$ to $\mathcal{I}_5$ for $D = D_7$, then from $\mathcal{I}_5$ to $\mathcal{I}_4$ for $D = D_6$, then from $\mathcal{I}_4$ to $\mathcal{I}_3$ for $D = D_3$, then from $\mathcal{I}_3$ to $\mathcal{I}_0$ for $D = D_4$. The bifurcation values D_3, D_4, D_6 and D_7 are given in Table 9. The bifurcation value D_4 corresponds to a transcritical bifurcation of E_2^0 and E_1^0; D_3 corresponds to a transcritical bifurcation of E_2^1 and E_2^0 and D_6 and D_7 correspond to transcritical bifurcations of E_2^0 and E_2^2. The plot of X_1 and X_2 components of all existing steady states with respect of D is shown in Fig. 10. Solid lines and dotted lines correspond to stable and unstable steady states respectively. On Fig. 10(a), for $0 < D < D_7$ and $D_6 < D < D_5$ the X_1-component of E_2^i, $i = 0, 2$, is colored in Red, with Green dots, showing the stability of E_2^1 and the instability of E_2^0. For $D_7 < D < D_6$, the X_1-component of E_2^i, $i = 0, 1, 2$, is colored in Red and Green, with Blue dots, showing the bistability of E_2^0 and E_2^1 and the instability of E_2^1. For $D_3 < D < D_4$, the X_1-component of E_2^0 is colored in Green, showing the stability of E_2^0. On Fig. 10(b) and 10(c), for $0 < D < D_7$

and $D_6 < D < D_3$, the $X_2 = 0$-component of E_j^0, $j = 1, 2$, is colored with Green and Black dots, showing the instability of E_2^0 and E_1^0. For $D_7 < D < D_6$ and $D_3 < D < D_4$ it is colored in Green, with Black dots, showing the stability of E_2^0 and the instability of E_1^0. For $D > D_4$ it is colored in Black showing the stability of E_1^0.

Consider now the case where $S_{1\text{in}} = 13.3$. This case corresponds also to the situation where we can go from the bistability region (colored in Pink) to the global asymptotic stability region (colored in Green), when the dilution rate D increases. Since $13.11 < S_{1\text{in}} < 13.37$, as it is seen in Fig. 8, with increasing D, there is a transition from $\mathcal{I}_4$ to $\mathcal{I}_5$ for $D = D_{10}$, then from $\mathcal{I}_5$ to $\mathcal{I}_4$ for $D = D_9$, then from $\mathcal{I}_4$ to $\mathcal{I}_5$ for $D = D_8$, then from $\mathcal{I}_5$ to $\mathcal{I}_3$ for $D = D_2$, then from $\mathcal{I}_3$ to $\mathcal{I}_0$ for $D = D_4$. The bifurcation values D_2, D_4, D_8, D_9 and D_{10} are given in Table 9. The bifurcation value D_4 corresponds to a transcritical bifurcation of E_2^0 and E_1^0; D_2 corresponds to a saddle node bifurcation of E_2^1 and E_2^2 and D_8, D_9 and D_{10} correspond to transcritical bifurcations of E_2^0 and E_2^2. The plot of the X_2 component of all existing steady states with respect of D is shown in Fig. 11. Solid lines and dotted lines correspond to stable and unstable steady states respectively. Since two magnifications are necessary to represent all bifurcations, the plot of the X_1 component is omitted in Fig. 11. However, it is similar to those plots given in Figs. 9(a) and 10(a). On Fig. 11 for $0 < D < D_{10}$ and $D_9 < D < D_8$, the $X_2 = 0$-component of E_j^0, $j = 1, 2$, is colored with Green and Black dots, showing the instability of E_2^0 and E_1^0; For $D_{10} < D < D_9$ and $D_8 < D < D_4$ it is colored in Green, with Black dots, showing the stability of E_2^0 and the instability of E_1^0. For $D > D_4$ it is colored in Black showing the stability of E_1^0. Notice that for $D_{10} < D < D_9$ and $D_8 < D < D_2$ both steady states E_2^0 and E_2^1 are stable.

7 Discussion

The parameter space of model (2), where μ_1 and μ_2 are given by (3) is twelve dimensional: nine biological and physical parameters (m_1, m_2, K_1, K_2,K_I, k_1, k_2, k_3 and α) and three operating parameters (D, $S_{1\text{in}}$ and $S_{2\text{in}}$). The former parameters are called biological parameters since they depend on the organisms, and substrate considered. These parameters are measurable in the laboratory, using ecological and biological observations. In contrast, the later parameters are called operating parameters since they are under the control of the experimenter.

Exploring all of the twelve dimensional parameter space is almost possible. Fixing the biological parameters and constructing the operating diagram is a powerful answer for the discussion of the behavior of the model with respect of the parameters. Therefore our approach to handle the question of the dependence with respect of the parameters of the model is to split the question in two intermediary questions. First, we fix the biological parameters and present the operating diagram. Second, we explore how the operating diagram varies when the biological parameters are changed. For instance, Figs. 5, 6 and 7 show how the operating diagram changes when the biological parameter m_1 is changed.

The operating diagrams shown in the figures summarize the effect of the operating conditions on the long-term dynamics of the AM2 model and shows six type of behavior: 1) the washout of the two populations (regions colored in Red); 2) the washout of the first population while the second population is maintained (regions colored in Blue); 3) the occurrence of these two behaviors, according to initial conditions (regions colored in Cyan); 4) the washout of the second population while the first is maintained (regions colored in Yellow); 5) the persistence of both populations (regions colored in Green); 6) the occurrence of these two behaviors according to initial conditions (regions colored in Pink).

In the operating diagrams shown in Figs. 5(a), 6(a) and 7(a), obtained for $S_{2\text{in}} = 0$, only regions $\mathcal{I}_0$, $\mathcal{I}_3$, $\mathcal{I}_4$ and $\mathcal{I}_5$ exist, that is to say, the steady states E_1^i, $i = 1, 2$ without acidogenic bacteria, cannot exist. This property is in accordance with the fact that the system being commensalistic, and without input concentration $S_{2\text{in}}$, it is impossible for the commensal population (the methanogenic bacteria) to survive if the host population (the acidogenic bacteria) is washed out.

The operating diagram shows how robust or how extensive is the parameter region where coexistence occurs, where the corresponding steady state is GAS, where the steady states, with extinction of one or both populations, is stable and where it is unstable.

Our main contribution is to investigate the operating diagram and to show how it depends on the biological parameters. We have represented the three dimensional operating diagram in a series of two dimensional operating parameters space where the third parameter is kept fixed: In section 4, we presented operating diagrams in $(S_{1\text{in}}, S_{2\text{in}})$ plane, while D is fixed and in section 5, we fixed $S_{2\text{in}}$ and we gave operating diagrams in $(D, S_{1\text{in}})$ plane.

There are two other types of operating diagram representations that may be interesting for applications and will be the subject of a future article. We can also present the operating diagram in a series of diagrams

in $(D, S_{2\text{in}})$ with $S_{1\text{in}}$ fixed. This type of representation can be useful to the experimenter when the operating parameters $S_{2\text{in}}$ and D are those on which he can actually act, while the operating parameter $S_{1\text{in}}$ is more or less fixed. Another way of constructing the operating diagram is to consider a single input substrate $S_{\text{in}} = \alpha S_{1\text{in}} + (1-\alpha)S_{2\text{in}}$, with $0 \leq \alpha \leq 1$, and then to represent the operating diagram in the (S_{in}, D) plane by fixing α. This type of representation is used in the ADM1 model [8] or in the MAD model [17].

8 Conclusion

The two-step anaerobic digestion model, denoted AM2, was developed on the basis of macroscopic observations of anaerobic digestion processes and, widely fitted on experimental data and used for processes control by engineers. This model, when fitted accurately with experimental data, can be used by mathematicians to best understand and analyze the dynamics of the physical system (anaerobic digester) and, by biologists to predict future behavior of the system. The advantage of the mathematical analysis, compared to numerical simulation, is that the system can be studied in a generic way without specifying the values of the biological parameters. Therefore, the prediction of the mathematical analysis are true for a large class of values of the kinetic parameters. So, it is useful to build some roots for dialogue and discussion between the mathematical and biology communities. This paper proposed a powerful tool which can establish dialogue between the two communities: the operating diagram for two-step models similar to the AM2 model. We established a complete description of operating diagrams for the system with respect of the three operating parameters which are under the control of the experimenter: dilution rate (D) and substrates inflow concentrations ($S_{1\text{in}}$ and $S_{2\text{in}}$). We have represented the three dimensional operating diagram in a series of two dimensional operating parameters space where the third parameter is kept fixed. We have highlighted that this diagram, is very useful to describe the model from both the mathematical and biological points of view and to predict biological and ecological phenomena as coexistence of bacteria population or extinction of one or both of them. For instance, to know the behaviour of the system for a set of operating parameters $(D, S_{1\text{in}}, S_{2\text{in}})$, we can construct the operating diagram $(S_{1\text{in}}, S_{2\text{in}})$, with D fixed at the value we are interested in, and see to which region $\mathcal{I}_k$, the operating parameter point $(S_{1\text{in}}, S_{2\text{in}})$ belongs. We can also construct the operating plane $(D, S_{1\text{in}})$, with $S_{2\text{in}}$ fixed at the value we are interested in, and see to which region $\mathcal{I}_k$, the operating parameter point $(D, S_{1\text{in}})$ belongs.

Biologists and experimenters can use the operating diagram to predict the long-term dynamics of the system and concentrations for bacteria and substrates at steady-state. Also when they act on the value of one operating parameter where the value of the other parameter is kept fixed, they can also explain and understand how the system goes from an operating region with two possible stable steady-states (bistability) to a region when the system has only one global stable steady-state, this is what the mathematicians call bifurcation. Another application showing why the presented operating diagrams are so important for experimenters is the system control. Indeed, by acting on the operating parameters D, $S_{1\text{in}}$ and $S_{2\text{in}}$, experimenters can control the behavior of the biological system and force it to converge towards a desired steady-state.

A Relationship to previous work

The two-step system (2) has been often consodered in the literature. As it is usual in the mathematical theory of the chemostat, see for instance [22], in this type of models, we can use a change of variables that reduces the pseudo-stoichiometric coefficients k_i to 1. Indeed, the linear change of variables

$$s_1 = (k_2/k_1)S_1, \quad x_1 = k_2 X_1, \quad s_2 = S_2, \quad x_2 = k_3 X_2,$$

transforms (2) into

$$\begin{array}{l} \dot{s}_1 = D\,(s_{1\text{in}} - s_1) - f_1\,(s_1)\,x_1, \\ \dot{x}_1 = (f_1\,(s_1) - \alpha D)\,x_1, \\ \dot{s}_2 = D\,(s_{2\text{in}} - s_2) + f_1\,(s_1)\,x_1 - f_2\,(s_2)\,x_2, \\ \dot{x}_2 = (f_2\,(s_2) - \alpha D)\,x_2, \end{array} \tag{4}$$

where

$$s_{1\text{in}} = (k_2/k_1)S_{1\text{in}}, \quad s_{2\text{in}} = S_{2\text{in}},$$
$$f_1(s_1) = \mu_1\left((k_1/k_2)s_1\right), \quad f_2(s_2) = \mu_2(s_2).$$

However, since the stoichiometric coefficients have their own importance for the biologist and since we are interested in giving these later a useful tool for the understanding of the role of the operating parameters, following [6], we do not make this reduction and we present the results in the original model (2). This model can have at most six steady states, labeled below as in [6]:

- E_1^0, where $X_1 = 0$ and $X_2 = 0$: the washout steady state where acidogenic and methanogenic bacteria are extinct.
- E_1^i $(i = 1, 2)$, where $X_1 = 0$ and $X_2 > 0$: acidogenic bacteria are washed out, while methanogenic bacteria are maintained.
- E_2^0, where $X_1 > 0$ and $X_2 = 0$: methanogenic bacteria are washed out, while acidogenic bacteria are maintained.
- E_2^i $(i = 1, 2)$, where $X_1 > 0$ and $X_2 > 0$: both acidogenic and methanogenic bacteria are maintained.

As shown in Proposition 1 of [6], the components of the steady states E_1^0, E_1^i $(i = 1, 2)$, E_2^0 and E_2^i $(i = 1, 2)$ are given in Table 2, where S_1^*, S_2^{i*}, $S_{2\text{in}}^*$, X_1^*, X_2^i, and X_2^{i*}, for $i = 1, 2$, are defined in Table1. The necessary and sufficient conditions of existence of the steady states, given in Proposition 1 of

Table 10 Necessary and sufficient conditions of existence and local stability of the steady states of (2) obtained in [6]. $S_1^*(D)$, $S_2^{i*}(D)$ and $S_{2\text{in}}^*(D, S_{1\text{in}}, S_{2\text{in}})$ are defined in Table 1.

	Existence conditions	Stability conditions
E_1^0	Always exists	$S_{1\text{in}} < S_1^*(D)$ and $S_{2\text{in}} \notin [S_2^{1*}(D), S_2^{2*}(D)]$
E_1^1	$S_{2\text{in}} > S_2^{1*}(D)$	$S_{1\text{in}} < S_1^*(D)$
E_1^2	$S_{2\text{in}} > S_2^{2*}(D)$	Unstable if it exists
E_2^0	$S_{1\text{in}} > S_1^*(D)$	$S_{2\text{in}}^*(D, S_{1\text{in}}, S_{2\text{in}}) \notin [S_2^{1*}(D), S_2^{2*}(D)]$
E_2^1	$S_{1\text{in}} > S_1^*(D)$ and $S_{2\text{in}}^*(D, S_{1\text{in}}, S_{2\text{in}}) > S_2^{1*}(D)$	Stable if it exists
E_2^2	$S_{1\text{in}} > S_1^*(D)$ and $S_{2\text{in}}^*(D, S_{1\text{in}}, S_{2\text{in}}) > S_2^{2*}(D)$	Unstable if it exists

Table 11 The 9 cases of existence and stability of steady states of (2) obtained in [6], and the corresponding regions defined in Table 5.

Condition 1	Condition 2	Case	Region	E_1^0	E_1^1	E_1^2	E_2^0	E_2^1	E_2^2
$S_{1\text{in}} < S_1^*(D)$	$S_{2\text{in}} < S_2^{1*}(D)$	**1.1**	$\mathcal{I}_0$	S					
	$S_2^{1*}(D) < S_{2\text{in}} \leq S_2^{2*}(D)$	**1.2**	$\mathcal{I}_1$	U	S				
	$S_2^{2*}(D) < S_{2\text{in}}$	**1.3**	$\mathcal{I}_2$	S	S	U			
$S_{1\text{in}} > S_1^*(D)$	$S_{2\text{in}} < S_{2\text{in}}^* < S_2^{1*} < S_2^{2*}$	**2.1**	$\mathcal{I}_3$	U			S		
	$S_{2\text{in}} \leq S_2^{1*} < S_{2\text{in}}^* \leq S_2^{2*}$	**2.2**	$\mathcal{I}_4$	U			U	S	
	$S_{2\text{in}} \leq S_2^{1*} < S_2^{2*} < S_{2\text{in}}^*$	**2.3**	$\mathcal{I}_5$	U			S	S	U
	$S_2^{1*} < S_{2\text{in}} < S_{2\text{in}}^* \leq S_2^{2*}$	**2.4**	$\mathcal{I}_6$	U	U		U	S	
	$S_2^{1*} < S_{2\text{in}} \leq S_2^{2*} < S_{2\text{in}}^*$	**2.5**	$\mathcal{I}_7$	U	U		S	S	U
	$S_2^{1*} < S_2^{2*} < S_{2\text{in}} < S_{2\text{in}}^*$	**2.6**	$\mathcal{I}_8$	U	U	U	S	S	U

[6], are summarized in the second column of Table 10. The necessary and sufficient conditions of local stability of these steady states, obtained in Table A.1 of [6], are summarized in the third column of Table 10.

Remark 3 *In Table 10, since the function S_1^* is defined on $(0, D_1)$, the condition $S_{1\text{in}} > S_1^*(D)$ means $0 < D < D_1$ and $S_{1\text{in}} > S_1^*(D)$. Conversely, since by convention $S_1^*(D) = +\infty$ for $D \geq D_1$, the condition $S_{1\text{in}} < S_1^*(D)$ means $D \geq D_1$ and $S_{1\text{in}} > 0$ or $0 < D < D_1$ and $0 < S_{1\text{in}} < S_1^*(D)$. On the other hand, since the function S_2^{i*} is defined on $(0, D_2)$, the condition $S_{2\text{in}} > S_2^{i*}(D)$ means $0 < D < D_2$ and $S_{2\text{in}} > S_2^{i*}(D)$ and, conversely, since by convention $S_2^{1*}(D) = +\infty$ for $D > D_2$, the condition $S_{2\text{in}} \notin [S_2^{1*}(D), S_2^{2*}(D)]$ means $D \geq D_2$ and $S_{2\text{in}} > 0$ or $0 < D < D_2$ and*

$$S_{2\text{in}} \notin \left[S_2^{1*}(D), S_2^{2*}(D)\right].$$

The existence and stability conditions of the steady states of (2) given in Table 10 depend only on the relative positions of the values of S_{1in} and $S_1^*(D)$ and of the values of

$$S_2^{1*}(D),\ S_2^{2*}(D),\ S_{2in} \text{ and } S_{2in}^*(D, S_{1in}, S_{2in}).$$

Actually, as stated in Theorem 1 of [6], we can distinguish nine cases, according to the relative positions of these numbers. These cases are summarized in Table 11, together with the corresponding regions $\mathcal{I}_k$, $k = 0, \cdots, 8$ of Table 5.

Remark 4 *Note that Table 10 is identical to Table 3, except for the stability condition of E_2^0, and the existence conditions of E_2^{i*}, $i = 1, 2$, which are expressed in Table 3 using the H_i, $i = 1, 2$, functions, defined in Table 1.*

Let us prove the following lemma which shows that the existence conditions of E_2^{i*}, $i = 1, 2$, given in Table 10, can be stated using the functions $H_i(D)$, defined in Table 1.

Lemma 1 *The conditions $S_{2\text{in}}^*(D, S_{1\text{in}}, S_{2\text{in}}) = S_2^{i*}(D)$ and $S_{2\text{in}}^*(D, S_{1\text{in}}, S_{2\text{in}}) < S_2^{i*}(D)$, for $i = 1, 2$, are equivalent to the conditions $S_{2\text{in}} + \frac{k_2}{k_1} S_{1\text{in}} = H_i(D)$ and $S_{2\text{in}} + \frac{k_2}{k_1} S_{1\text{in}} < H_i(D)$, for $i = 1, 2$, respectively.*

Proof The result follows from the definitions of the functions $S_{2\text{in}}^*(D, S_{1\text{in}}, S_{2\text{in}})$ and $H_i(D)$, given in Table 1. Indeed, the condition $S_{2\text{in}}^*(D, S_{1\text{in}}, S_{2\text{in}}) = S_2^{i*}(D)$ is equivalent to:

$$S_{2\text{in}} + \frac{k_2}{k_1}\left(S_{1\text{in}} - S_1^*(D)\right) = S_2^{i*}(D),$$

which is itself equivalent to :

$$S_{2\text{in}} + \frac{k_2}{k_1} S_{1\text{in}} = S_2^{i*}(D) + \frac{k_2}{k_1} S_1^*(D).$$

That is to say $S_{2\text{in}} + \frac{k_2}{k_1} S_{1\text{in}} = H_i(D)$. The proof for the inequality is the same.

The role of H_i-functions, in the description of the operating diagram, has already been highlighted, see Fig. 4 in [25], where cases $D_2 < D_1$ and $D_1 < D_2$ are distinguished.

B Proofs

B.1 Proof of Proposition 1

It is seen from Proposition 1 of [6] that the steady states are given by Table 2, where S_1^*, S_2^{i*}, $S_{2\text{in}}^*$, X_1^*, X_2^i and X_2^{i*} are defined in Table 1. Their conditions of existence and stability are given in Table 10. Using Lemma 1 it is seen that the results in Table 10 are equivalent to those in Table 3 which completes the proof of Proposition 1.

B.2 Proof of Proposition 2

The cases **1.1**, **1.2** and **1.3** correspond to the regions $\mathcal{I}_0$, $\mathcal{I}_1$ and $\mathcal{I}_2$ respectively, defined in Table 5. Now we use Lemma 1 to show that the remaining six cases **2.1** to **2.6** correspond to the six regions $\mathcal{I}_3$ to $\mathcal{I}_8$ defined in Table 5.

Since $S_{2\text{in}} < S^*_{2\text{in}}$ the case **2.1** corresponds to the condition $S^*_{2\text{in}} < S_2^{1*}$ which is equivalent, using Lemma 1, to

$$S_{2\text{in}} + \frac{k_2}{k_1} S_{1\text{in}} < H_1(D).$$

Therefore the case **2.1** corresponds to the region $\mathcal{I}_3$ defined in Table 5. Using again Lemma 1, the condition $S_2^{1*} < S^*_{2\text{in}} < S_2^{2*}$ in the case **2.2** is equivalent to

$$H_1(D) < S_{2\text{in}} + \frac{k_2}{k_1} S_{1\text{in}} < H_2(D)$$

and the condition $S^*_{2\text{in}} > S_2^{2*}$ in the case **2.3** is equivalent to

$$S_{2\text{in}} + \frac{k_2}{k_1} S_{1\text{in}} > H_2(D).$$

Therefore the cases **2.2** and **2.3** correspond to the regions $\mathcal{I}_4$ and $\mathcal{I}_5$ respectively, defined in Table 5. Using similar arguments we show that the cases **2.4**, **2.5** and **2.6** correspond to the regions $\mathcal{I}_6$, $\mathcal{I}_7$ and $\mathcal{I}_8$ respectively, defined in Table 5.

Excepted for cases **1.3**, **2.3**, **2.5** and **2.6** of bistability, the system (2) has a unique globally asymptotically stable (GAS) steady state. Therefore, in the case **1.1**, E_1^0 is GAS; in the case **1.2**, E_1^1 is GAS, in the case **2.1**, E_2^0 is GAS, and in the cases **2.2** and **2.4**, E_2^1 is GAS. In the case **1.3**, E_1^2 is a saddle point whose attractive manifold is a 3-dimensional hyper-surface surface which separates the phase space of (2) into the basins of attractions of the stable steady states E_1^0 and E_1^1. In the cases **2.3**, **2.5** and **2.6**, E_2^2 is a saddle point whose stable manifold is a 3-dimensional hyper-surface which separates the phase space of (2) into the basins of attractions of the stable steady states E_2^0 and E_2^1. For details and complements on the global behaviour, see section 2.4 of [6]. This completes the proof of Proposition 2.

B.3 Proof of Proposition 3

Part of the proof follows from [6]. It is seen from Theorem 1 of [6] that *non hyperbolic* steady states, that correspond to coalescence of some of the steady state, occur when two (or more) of the values of $S_2^{1*}(D)$, $S_2^{2*}(D)$, S_{2in}, and $S^*_{2in}(D, S_{1in}, S_{2in})$ are equal. Notice that the condition

$$S_2^{1*}(D) = S_2^{2*}(D),$$

arising in cases **1.6**, **2.11** and **2.14** of Theorem 1 of [6], corresponds of the saddle node bifurcations of $E_1^1 = E_1^2$ or $E_2^1 = E_2^2$. This condition holds on Γ_6,

Notice the condition $S_{2\text{in}} = S_2^{1*}(D)$, arising in cases **1.4**, **2.8** and **2.9** of Theorem 1 of [6], corresponds of the transcritical bifurcation $E_1^0 = E_1^1$. This condition holds on Γ_2. Similarly, the condition $S_{2\text{in}} = S_2^{2*}(D)$, arising in cases **1.5** and **2.13** of Theorem 1 of [6], corresponds of the transcritical bifurcation $E_1^0 = E_1^2$. This condition holds on Γ_3.

On the other hand the condition $S^*_{2\text{in}} = S_2^{1*}(D)$, arising in cases **2.7** of Theorem 1 of [6], corresponds of the transcritical bifurcation $E_2^0 = E_2^1$. Using Lemma 1, this condition holds on Γ_4. Similarly, the condition $S^*_{2\text{in}} = S_2^{2*}(D)$, arising in cases **2.12** and **2.15** of Theorem 1 of [6], corresponds of the transcritical bifurcation $E_2^0 = E_2^2$. Using Lemma 1, this condition holds on Γ_5.

Finally we consider the bifurcations occurring when $S_{1\text{in}} = S_1^*(D)$. These bifurcations were not considered in Theorem 1 of [6]. The condition $S_{1\text{in}} = S_1^*(D)$ holds on Γ_1 and corresponds to the transcritical bifurcations $E_1^0 = E_2^0$, $E_1^1 = E_2^1$ and $E_1^2 = E_2^2$. This completes the proof of Proposition 3.

C Maple code

All plots in this paper were performed with Maple. For the convenience of the reader we give hereafter the Maple instructions to plot Figs. 5, 6 and 7. The table 12 gives explicitly the functions used in the definitions of the Γ_i curves in 14. The plots of these curves is obtained as follows.

```
restart;#How to plot Figs. 5, 6 and 7
with(plots):
S1star:= alpha*D*K1/(m1-alpha*D):
Delta:=(m2-alpha*D)^2*Ki^2-4*(alpha*D)^2*K2*Ki:
S21star:=(Ki*(m2-alpha*D)-sqrt(Delta))/(2*alpha*D):
S22star:=(Ki*(m2-alpha*D)+sqrt(Delta))/(2*alpha*D):
H1:=S21star+k2*S1star/k1:
H2:=S22star+k2*S1star/k1:
S2M:=sqrt(K2*Ki): mu2M:=m2/(1+2*sqrt(K2/Ki)):
D1:=m1/alpha: D2:=mu2M/alpha:
C:=subs(D=D2,S1star)+k1*(S2M-S2in)/k2:
#Parameter values;
K1:=2.1: m2:=0.95: K2:=24: Ki:=55: alpha:=0.5:
k1:=25: k2:=250:  k3:=268:
m1:=0.6:# Corresponds to Fig. 5
Dm:=1.2: Sm:=15: # Range of plot
#Plot of Fig. 12(a)
S2in:=0;
Gamma1:=plot(S1star,D=0..Dm,0..Sm,color=blue):
Gamma4:=plot(k1*(H1-S2in)/k2,D=0..D2,0..Sm,color=red):
Gamma5:=plot(k1*(H2-S2in)/k2,D=0..D2,0..Sm,color=red):
Gamma6:=plot([D2,S,S=C..Sm],D=0..Dm,0..Sm,color=black):
display(Gamma1,Gamma4,Gamma5,Gamma6);
#Plot of Fig. 12(b)
S2in:=15;
D0:=solve(S21star=S2in):
Gamma2:=plot([D0,S,S=0..Sm],0..Dm,0..Sm,color=green):
Gamma1:=plot(S1star,D=0..Dm,0..Sm,color=blue):
Gamma4:=plot(k1*(H1-S2in)/k2,D=D0..D2,0..Sm,color=red):
Gamma5:=plot(k1*(H2-S2in)/k2,D=0..D2,0..Sm,color=red):
Gamma6:=plot([D2,S,S=C..Sm],D=0..Dm,0..Sm,color=black):
display(Gamma2,Gamma1,Gamma4,Gamma5,Gamma6);
#Plot of Fig. 12(c)
S2in:=S2M;
Gamma2:=plot([D2,S,S=0..Sm],0..Dm,0..Sm,color=green):
Gamma1:=plot(S1star,D=0..Dm,0..Sm,color=blue):
Gamma5:=plot(k1*(H2-S2in)/k2,D=0..D2,0..Sm,color=red):
display(Gamma2,Gamma1,Gamma5);
#Plot of Fig. 12(d)
S2in:=100;
D0:=solve(S22star=S2in):
Gamma2:=plot([D0,S,S=0..Sm],0..Dm,0..Sm,color=green):
Gamma1:=plot(S1star,D=0..Dm,0..Sm,color=blue):
Gamma5:=plot(k1*(H2-S2in)/k2,D=0..D0,0..Sm,color=red):
Gamma6:=plot([D2,S,S=0..Sm],D=0..Dm,0..Sm,color=black):
display(Gamma2,Gamma1,Gamma5,Gamma6);
```

The Γ_i curves and the $\mathcal{I}_k$ regions they delimit are shown in Fig. 12. This figure is identical to Fig. 5, except that in

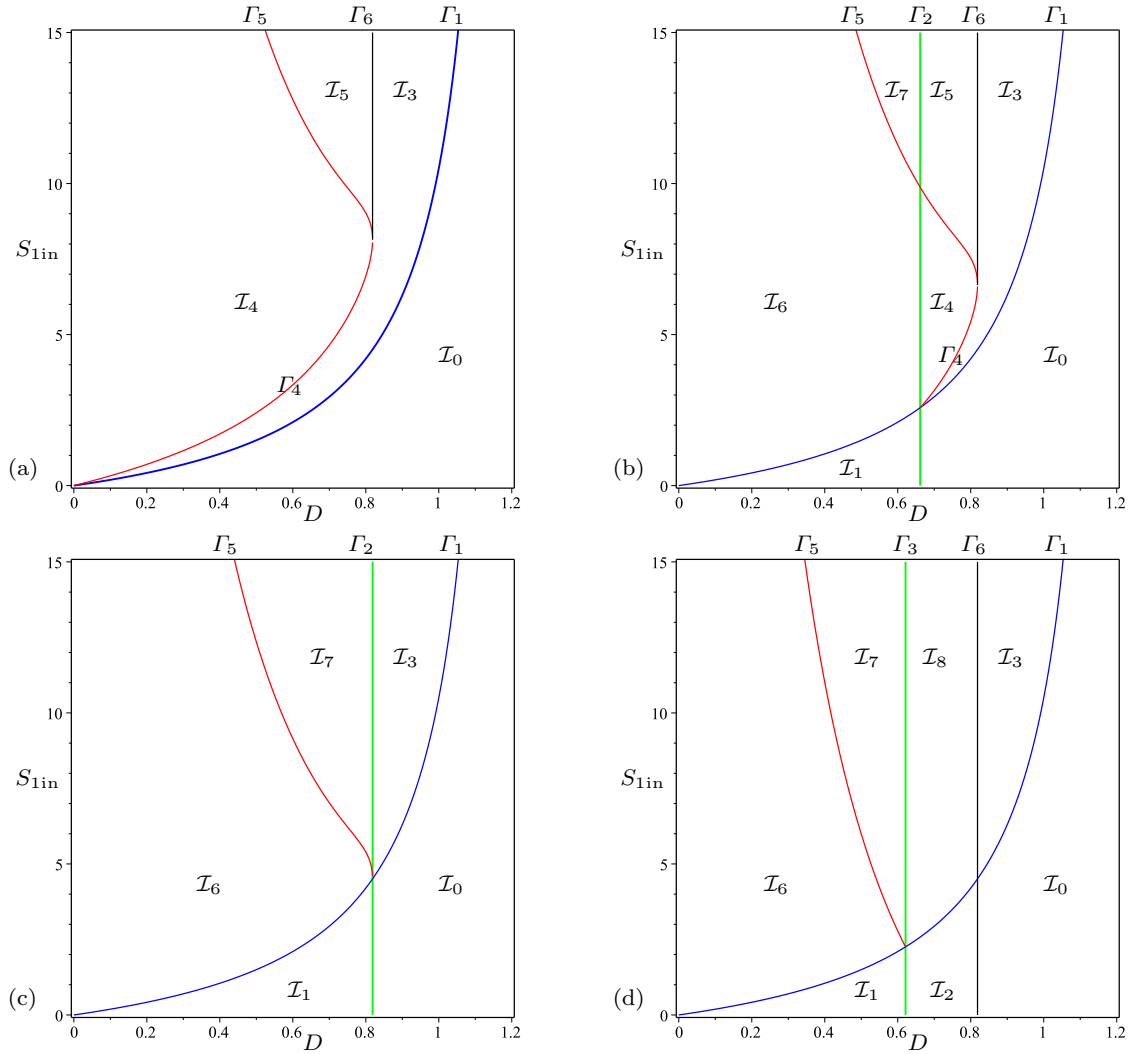

Fig. 12 The curves Γ_1 (in Blue), Γ_2 and Γ_3 (in Green), Γ_4 and Γ_5 (in Red) and Γ_6 (in Black), corresponding to the operating diagrams in Fig. 5. (a): $S_{2\text{in}} = 0$, (b): $S_{2\text{in}} = 15$, (c): $S_{2\text{in}} = S_2^M \simeq 36.332$ and (d): $S_{2\text{in}} = 100$.

Fig. 5, the regions $\mathcal{I}_k$ have been colored using the colors of Table 6.

D Tables and three dimensional operating diagram

In this section, we give several tables that are used in the paper. In the table 12, we present the functions defined in the table 1, in the particular case of the growth functions of Monod and Haldane (3). Tables 13 and 14, give the description of the intersections with a two dimensional operating plane, where D or S_{2in} is kept constant, respectively, of the Γ_i surfaces that separate the operating parameter space in several regions, which are defined in Table 4. In Table 15, we provide the biological parameter values of the Monod and Haldane growth functions (3) used in the figures.

For the biological parameter values given in Table 15, and $m_1 = 0.6$, we give in Fig. 13 front, rear, left and right views of the surfaces Γ_i, $i = 1, \cdots, 6$, in the three dimensional operating space, showing the various regions of the three dimensional operating diagram. In this three-dimensional view, the surfaces Γ_i are colored as in Fig. 12, except that, for clarity, Γ_6 is colored yellow, rather than black.

Acknowledgements The authors thank the two anonymous reviewers for their constructive comments which have greatly improved this work. The authors thank Jérôme Harmand for valuable and fruitful discussions. The authors thank the Euro-Mediterranean research network Treasure (`http://www.inra.fr/treasure`) and the Direction Générale de la Recherche Scientifique et du Développement Technologique, Algeria, for support. Part of the work was completed during the mission of the second author in Narbonne. This mission was publicly funded through ANR (the French National Research Agency) under the "Investissements d'avenir" programme with the reference ANR-16-IDEX-0006.

Conflict of interest

The authors declare that they have no conflict of interest.

Table 12 Auxiliary functions in the case given by (3).

$\mu_1(S_1) = \dfrac{m_1 S_1}{K_1 + S_1}$, $\mu_1(+\infty) = m_1$
$S_1^*(D) = \dfrac{\alpha D K_1}{m_1 - \alpha D}$. It is defined for $0 < D < D_1$, where $D_1 = \dfrac{m_1}{\alpha}$
$\mu_2(S_2) = \dfrac{m_2 S_2}{K_2 + S_2 + \frac{S_2^2}{K_I}}$, $S_2^M = \sqrt{K_2 K_I}$, $\mu_2(S_2^M) = \dfrac{m_2}{1 + 2\sqrt{K_2/K_I}}$
$S_2^{1*}(D) = \dfrac{(m_2 - \alpha D)K_I - \sqrt{(m_2 - \alpha D)^2 K_I^2 - 4(\alpha D)^2 K_2 K_I}}{2\alpha D}$
$S_2^{2*}(D) = \dfrac{(m_2 - \alpha D)K_I + \sqrt{(m_2 - \alpha D)^2 K_I^2 - 4(\alpha D)^2 K_2 K_I}}{2\alpha D}$
$S_2^{1*}(D)$ and $S_2^{2*}(D)$ are defined for $0 < D < D_2$, where $D_2 = \dfrac{\mu_2(S_2^M)}{\alpha}$
$H_i(D) = S_2^{i*}(D) + \frac{k_2}{k_1} S_1^*(D)$, $i = 1, 2$, defined for $0 < D < \min(D_1, D_2)$
$S_{2\text{in}}^*(D, S_{1\text{in}}, S_{2\text{in}}) = S_{2\text{in}} + \frac{k_2}{k_1} S_{1\text{in}} - \frac{k_2}{k_1} S_1^*(D)$, defined for $0 < D < D_1$
$X_2^i(D, S_{2\text{in}}) = \frac{1}{k_3 \alpha}\left(S_{2\text{in}} - S_2^{i*}(D)\right)$, $i = 1, 2$, defined for $0 < D < D_2$
$X_2^{i*}(D, S_{1\text{in}}, S_{2\text{in}}) = \frac{1}{k_3 \alpha}\left(S_{2\text{in}} + \frac{k_2}{k_1} S_{1\text{in}} - \frac{k_2}{k_1} H_i(D)\right)$, $i = 1, 2$, defined for $0 < D < \min(D_1, D_2)$

Table 13 Intersections of the Γ_k surfaces, $k = 0, \cdots, 8$ with a $(S_{1\text{in}}, S_{2\text{in}})$ plane, where D is kept constant.

Γ_k	$\Gamma_k \cap \{D = \text{constant}\}$	
Γ_1	Vertical line $S_{1\text{in}} = S_1^*(D)$	if $D < D_1$
	Empty	if $D \geq D_1$
Γ_2	Horizontal line $S_{2\text{in}} = S_2^{1*}(D)$	if $D \leq D_2$
	Empty	if $D > D_2$
Γ_3	Horizontal line $S_{2\text{in}} = S_2^{2*}(D)$	if $D \leq D_2$
	Empty	if $D > D_2$
Γ_4	Oblique line $S_{2\text{in}} + \frac{k_2}{k_1} S_{1\text{in}} = H_1(D)$	if $D < \min(D_1, D_2)$
	Empty	if $D \geq \min(D_1, D_2)$
Γ_5	Oblique line $S_{2\text{in}} + \frac{k_2}{k_1} S_{1\text{in}} = H_2(D)$	if $D < \min(D_1, D_2)$
	Empty	if $D \geq \min(D_1, D_2)$
Γ_6	The whole plane	if $D = D_2$
	Empty	if $D \neq D_2$

Table 14 The intersections of the Γ_k surfaces, $k = 0, \cdots, 8$ with a $(D, S_{1\text{in}})$ plane, where $S_{2\text{in}}$ is kept constant.

Γ_k	$\Gamma_k \cap \{S_{2\text{in}} = \text{constant}\}$	
Γ_1	Curve of function $S_{1\text{in}} = S_1^*(D)$	
Γ_2	Vertical line $D = \frac{1}{\alpha}\mu_2(S_{2\text{in}})$	if $S_{2\text{in}} \leq S_2^M$
	Empty	if $S_{2\text{in}} > S_2^M$
Γ_3	Vertical line $D = \frac{1}{\alpha}\mu_2(S_{2\text{in}})$	if $S_{2\text{in}} \geq S_2^M$
	Empty	if $S_{2\text{in}} < S_2^M$
Γ_4	Curve of function $S_{1\text{in}} = \frac{k_1}{k_2}(H_1(D) - S_{2\text{in}})$ restricted to the domain $S_{1\text{in}} > S_1^*(D)$	
Γ_5	Curve of function $S_{1\text{in}} = \frac{k_1}{k_2}(H_2(D) - S_{2\text{in}})$ restricted to the domain $S_{1\text{in}} > S_1^*(D)$	
Γ_6	Vertical line $D = D_2$	

References

1. Alcaraz-González, V., Harmand, J., Rapaport, A., Steyer, J., González-Alvarez, V., Pelayo-Ortiz, C.: Software sensors for highly uncertain wwtps : a new approach based on interval observers. Water Res. **36**, 2515–2524 (2002). DOI 10.1016/S0043-1354(01)00466-3
2. Alcaraz-González, V., Harmand, J., Rapaport, A., Steyer, J., González-Alvarez, V., Pelayo-Ortiz, C.: Application of a robust interval observer to an anaerobic digestion process. Dev. Chem. Eng. Miner. Process **13**, 267–278 (2005). DOI 10.1002/apj.5500130308
3. Arzate, J.A., Kirstein, M., Ertem, F.C., Kielhorn, E., Ramirez, M.H., Neubauer, P., Cruz-Bournazou, M.N., Junne, S.: Anaerobic digestion model (AM2) for the description of biogas processes at dynamic feedstock loading rates. Chemie Ingenieur Technik **89**, 686–695 (2017). DOI 10.1002/cite.201600176
4. Batstone, D., Keller, J., Angelidaki, I., Kalyuzhnyi, S., Pavlostathis, S., Rozzi, A., Sanders, W., Siegrist, H.,

Table 15 Nominal parameters values used in [6] and corresponding to the figures.

Parameter Unit	m_1 d^{-1}	K_1 g/L	m_2 d^{-1}	K_2 mmol/L	K_I mmol/L	α	k_1	k_2 mmol/g	k_3 mmol/g
Case (A): Figs. 1(a)	0.6								
Case (B): Figs. 1(b)	0.5	2.1	0.95	24	55	0.5	25	250	268
Case (C): Figs. 1(c)	0.4								

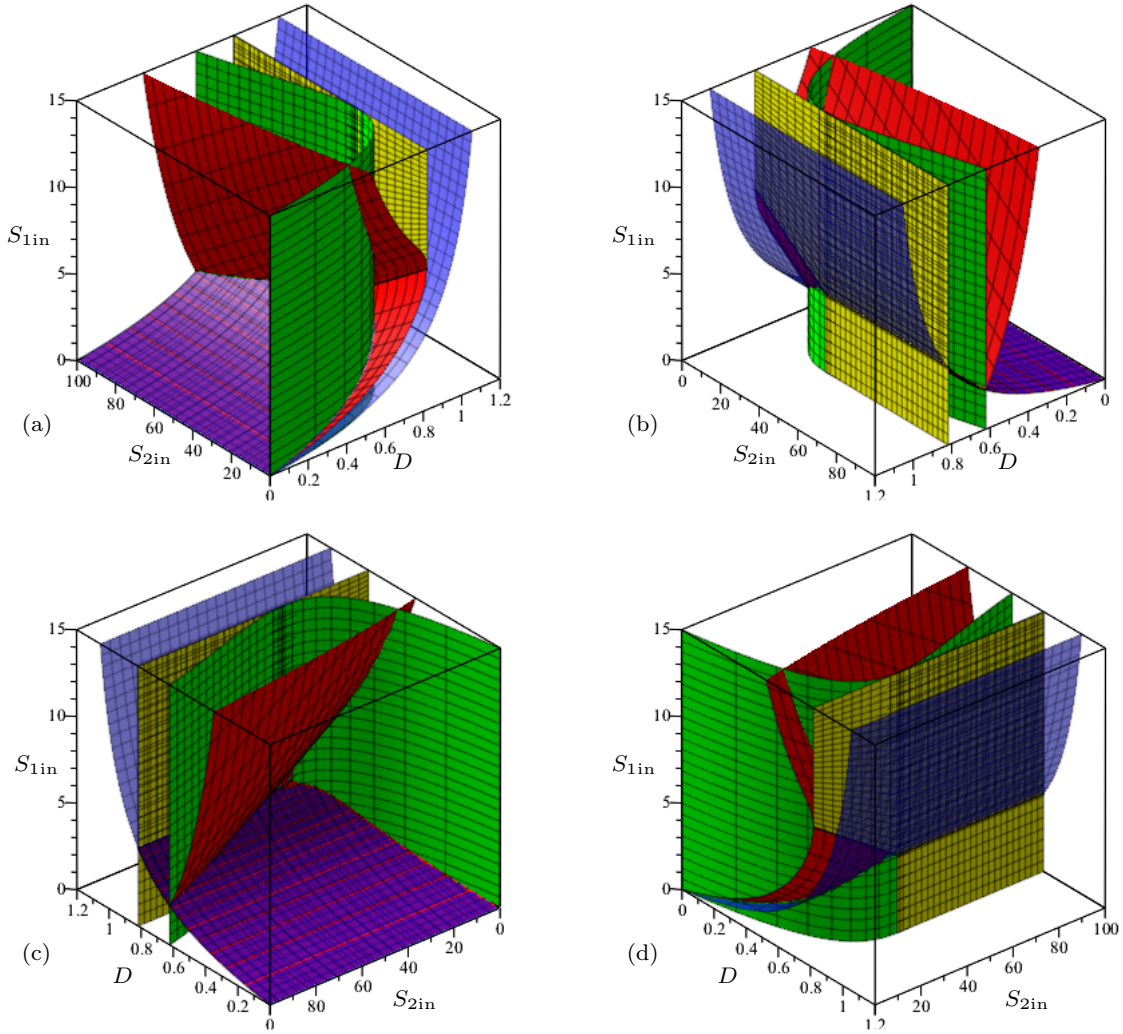

Fig. 13 The surfaces Γ_1 (in Blue), Γ_2 and Γ_3 (in Green), Γ_4 and Γ_5 (in Red) and Γ_6 (in Yellow), corresponding to Fig. 1(a). The surfaces separate the 3-dimensional operating space (D, S_{1in}, S_{2in}) in 9 regions $\mathcal{I}_k$, $k = 0, \cdots, 8$. Front (a), rear (b), left (c) and right (d) view of the surfaces Γ_i. Compare with Fig. 6 of [25].

Vavilin, V.: The IWA Anaerobic Digestion Model No 1 (ADM1). Water Sci Technol. **45**, 65–73 (2002). DOI 10.2166/wst.2002.0292

5. Bayen, T., Gajardo, P.: On the steady state optimization of the biogas production in a two-stage anaerobic digestion model. J. Math. Biol. **78**, 1067–1087 (2019). DOI 10.1007/s00285-018-1301-3

6. Benyahia, B., Sari, T., Cherki, B., Harmand, J.: Bifurcation and stability analysis of a two step model for monitoring anaerobic digestion processes. J. Process Control **22**, 1008–1019 (2012). DOI 10.1016/j.jprocont.2012.04.012

7. Bernard, O., Hadj-Sadock, Z., Dochain, D., Genovesi, A., Steyer, J.P.: Dynamical model development and parameter identification for an anaerobic wastewater treatment process. Biotechnol Bioeng. **75**, 424–438 (2001). DOI 10.1002/bit.10036

8. Bornhöft, A., Hanke-Rauschenbach, R., Sundmacher, K.: Steady-state analysis of the anaerobic digestion model no. 1 (adm1). Nonlinear Dynamics **73**, 535–549 (2013). DOI 10.1007/s11071-013-0807-x

9. Burchard, A.: Substrate degradation by a mutualistic association of two species in the chemostat. J. Math. Bio. **32**, 465–489 (1994). DOI 10.1007/BF00160169

10. Daoud, Y., Abdellatif, N., Sari, T., Harmand, J.: Steady state analysis of a syntrophic model: The effect of a new input substrate concentration. Math. Model. Nat. Phenom. **13**, 31 (2018). DOI 10.1051/mmnp/2018037
11. El-Hajji, M., Mazenc, F., Harmand, J.: A mathematical study of a syntrophic relationship of a model of anaerobic digestion process. Mathematical Biosciences & Engineering **7**, 641–656 (2010). DOI 10.3934/mbe.2010.7.641
12. García-Diéguez, C., Bernard, O., Roca, E.: Reducing the anaerobic digestion model no.1 for its application to an industrial wastewater treatment plant treating winery effluent wastewater. Bioresource Technology **132**, 244–253 (2013). DOI 10.1016/j.biortech.2012.12.166
13. Hanaki, M., Harmand, J., Mghazli, Z., Rapaport, A., Sari, T., Ugalde, P.: Mathematical study of a two-stage anaerobic model when the hydrolysis is the limiting step (2020). URL `https://hal.archives-ouvertes.fr/hal-02531141v2`. Preprint
14. Harmand, J., Lobry, C., Rapaport, A., Sari, T.: The Chemostat: Mathematical Theory of Microorganism Cultures. Wiley ISTE Editions (2017)
15. Harmand, J., Rapaport, A., Dochain, D.: Increasing the dilution rate can globally stabilize two-step biological systems. J. Process Control **95**, 67–74 (2020). DOI 10.1016/j.jprocont.2020.08.009
16. Jost, J., Drake, J., Fredrickson, A., Tsuchiya, H.: Interactions of *Tetrahymena pyriformis, Escherichia coli, Azotobacter Vinelandii*, and glucose in a minimal medium. J. Bacteriol. **113**, 834–840 (1973). URL `https://europepmc.org/article/pmc/pmc285298`
17. Khedim, Z., Benyahia, B., Cherki, B., Sari, T., Harmand, J.: Effect of control parameters on biogas production during the anaerobic digestion of protein-rich substrates. Applied Mathematical Modelling **61**, 351–376 (2018). DOI 10.1016/j.apm.2018.04.020
18. Meadows, T., Weedermann, M., Wolkowicz, G.S.K.: Global analysis of a simplified model of anaerobic digestion and a new result for the chemostat. SIAM J. Appl. Math. **79**, 668–689 (2019). DOI 10.1137/18M1198788
19. Monod, J.: La technique de culture continue. théorie et applications. Annales de l'Institut Pasteur **79**, 390–410 (1950). DOI 10.1016/B978-0-12-460482-7.50023-3
20. Pavlou, S.: Computing operating diagrams of bioreactors. J. Biotechnol. **71**, 7–16 (1999). DOI 10.1016/s0168-1656(99)00011-5
21. Reilly, P.: Stability of commensalistic systems. Biotechnology and Bioengineering **16**, 1373–1392 (1974). DOI 10.1002/bit.260161006
22. Sari, T., El-Hajji, M., Harmand, J.: The mathematical analysis of a syntrophic relationship between two microbial species in a chemostat. Math. Biosci. Eng. **9**, 627–645 (2012). DOI 10.3934/mbe.2012.9.627
23. Sari, T., Harmand, J.: A model of a syntrophic relationship between two microbial species in a chemostat including maintenance. Mathematical Biosciences **275**, 1–9 (2016). DOI 10.1016/j.mbs.2016.02.008
24. Sari, T., M.Wade: Generalised approach to modelling a three-tiered microbial food-web. Math. Biosci. **291**, 21–37 (2017). DOI 10.1016/j.mbs.2017.07.005
25. Sbarciog, M., Loccufier, M., Noldus, E.: Determination of appropriate operating strategies for anaerobic digestion systems. Biochemical Engineering Journal **51**, 80–188 (2010). DOI 10.1016/j.bej.2010.06.016
26. Shen, S., Premier, G., Guwy, A., Dinsdale, R.: Bifurcation and stability analysis of an anaerobic digestion model. Nonlinear Dynamics **48**, 465–489 (2007). DOI 10.1007/s11071-006-9093-1
27. Smith, H., Waltman, P.: The theory of the chemostat: Dynamics of microbial competition. Cambridge University Press (1995)
28. Stephanopoulos, G.: The dynamics of commensalism. Biotechnology and Bioengineering **23**, 2243–2255 (1981). DOI 10.1002/bit.260231008
29. Volcke, E.I.P., Sbarciog, M., Noldus, E.J.L., Baets, B.D., Loccufier, M.: Steady state multiplicity of two-step biological conversion systems with general kinetics. Mathematical Biosciences **228**, 160–170 (2010). DOI 10.1016/j.mbs.2010.09.004
30. Wade, M., Harmand, J., Benyahia, B., Bouchez, T., Chaillou, S., Cloez, B., Godon, J.J., Moussa-Boudjemaa, B., Rapaport, A., Sari, T., Arditi, R., Lobry, C.: Perspectives in mathematical modelling for microbial ecology. Ecological Modelling **321**, 64–74 (2016). DOI 10.1016/j.ecolmodel.2015.11.002
31. Wade, M., Pattinson, R., Parker, N., Dolfing, J.: Emergent behaviour in a chlorophenol-mineralising three-tiered microbial 'food web'. J. Theor. Biol. **389**, 171–186 (2016). DOI 0.1016/j.jtbi.2015.10.032
32. Wade, M.J.: Not just numbers: Mathematical modelling and its contribution to anaerobic digestion processes. Processes **8**(8) (2020). DOI 10.3390/pr8080888. URL `https://www.mdpi.com/2227-9717/8/8/888`
33. Weedermann, M., Seo, G., Wolkowics, G.S.K.: Mathematical model of anaerobic digestion in a chemostat: Effects of syntrophy and inhibition. Journal of Biological Dynamics **7**, 59–85 (2013). DOI 10.1080/17513758.2012.755573
34. Weedermann, M., Wolkowicz, G.S.K., Sasara, J.: Optimal biogas production in a model for anaerobic digestion. Nonlinear Dynamics **81**, 1097–1112 (2015). DOI 10.1007/s11071-015-2051-z
35. Xu, A., Dolfing, J., Curtis, T., Montague, G., Martin, E.: Maintenance affects the stability of a two-tiered microbial 'food chain'? J. Theor. Biol. **276**, 35–41 (2011). DOI 10.1016/j.jtbi.2011.01.026